Dielectrophoretic Trapping and Raman Spectroscopy of Fluorescent Oligonucleotides

Ville Ari

Master's Thesis
University of Jyväskylä, Department of Physics
September 14, 2016
Supervisors: Jussi Toppari
Janne Ihalainen

Preface

The experimental work for this Master's thesis has been conducted at the Nanoscience Center of the Department of Physics in the University of Jyväskylä during 2011.

Foremost I would like to thank my supervisors Dr. Jussi Toppari and Professor Janne Ihalainen for their guidance and the opportunity to work on this subject. Their patience with me has been commendable. Secondly I would like to thank Dr. Veikko Linko and M.Sc. Shen Boxuan for teaching me the use of the cleanroom equipment needed for this work. I am also grateful for all the other NSC personnel who have helped me in any way. I also want to thank my family and my friends, especially Dr. Janne Nevalaita, M.Sc. Vesa Pitkänen, M.Sc. Mauri Jauhiainen and Mr. Joonas Nevalaita for their friendship and support during my studies.

Jyväskylä, November 22, 2016

Ville Ari

Abstract

The purpose of this study was to see if 40 bp poly-CT DNA oligonucleotides modified with a thiol group and a Cy3 dye molecule trapped on a silicon oxide surface using dielectrophoresis could be detected under a Raman microscope. Obtaining a clear Raman signal proved to be challenging though and in the end the only peaks visible in the Raman spectra were those originating from the silicon substrate. There were problems with the confocal fluorescence microscope too. The bad alignment of its lasers made the task of acquiring proper images rather difficult. The spatial resolution of the Raman setup was known to be in the micron scale at least but not probably extending to hundreds of nano metres. Therefore the result was somewhat expected. A successful Raman detection would have been a positive note in the search of label free imaging techniques for biosciences.

Tiivistelmä

Nanotiede kasvaa edelleen tutkimusalana nopeasti, ja sille löytyy lukematon määrä sovelluskohteita. Sen vahvuutena on poikkitieteellisyys fysiikan, kemian ja biologian kesken, jotka kaikki tutkivat atomitason ilmiöitä. Näiden ilmiöiden tutkiminen ja soveltaminen vaatii paljon erilaisia, sofistikoituneita menetelmiä ja työkaluja, joilla voidaan valmistaa ja karakterisoida erilaisia nanopartikkeleita ja -rakenteita. Joissain tapauksissa vaaditaan jopa yksittäisten molekyylien tai atomien manipulointia nanometritasolla.

DNA on yksi mielenkiintoisista nanotieteen tutkimuskohteista. Se on elämän kannalta merkittävä molekyyli, sillä se pitää sisällään elävän organismin rakenteellisen ohjeen. DNA:n tärkeä rooli proteiinisynteesissä vaatii sen olevan kemiallisesti erittäin vakaa ja tarkasti hallittava. Nämä ominaisuudet tekevät siitä monipuolisen ja tärkeän tutkimuskohteen. DNA:n itsejärjestyvyysominaisuuksien takia sen käyttöä erilaisina ohjelmoitavina rakennuspalikoina ja tukirakenteina on tutkittu innokkaasti. Pii-pohjaisen mikro- ja nanopiiritekniikan suorituskyvyn lähestyessä fysikaalisia rajojaan myös DNA:n sähkönjohtavuutta on tutkittu mahdollisten nanoelektroniikkaan liittyvien sovellusten takia.

DNA:n hyödyntämisen mahdollistaa sen muokattavuus. DNA-oligonukleotidit ovat synteettisiä, yleensä muutaman kymmenen emäsparin pituisia yksijuosteisia DNA-molekyylejä, joihin voi valita mieleisensä sekvenssin sovelluskohteen mukaan. Molekyylin molempiin päihin on myös mahdollista liittää erilaisia funktionaalisia molekyylejä. Tämä ominaisuus on hyödyllinen erityisesti biotieteissä, joissa hyödynnetään paljon fluoresenssimikroskopiaa. Koska näytteet eivät aina ole itsessään fluoresoivia, ne täytyy tarvittaessa leimata tilanteeseen sopivilla merkkiaineilla. Lisäksi koejärjestelystä riippuen voidaan tarvita esimerkiksi erilaisia linkkeri-molekyylejä.

Erilaisten molekulaaristen modifikaatioiden käyttöön kuvantamisessa liittyy kuitenkin se heikkous, että ne lisäävät näytteiden monimutkaisuutta ja hintaa. Siten kuvantamistekniikat, joiden käyttö ei vaadi erillisiä merkkiaineita, voivat joissain tapauksissa olla suureksi hyödyksi. Raman-spektroskopia, esimerkiksi, perustuu sähkömagneettisen säteilyn Raman-sirontaan fluoresenssin sijaan.

Intialaiset fyysikot *C. V. Raman* ja *K. S. Krishnan* todistivat sen olemassaolon 1920-luvun alussa. Valo voi elastisen Rayleigh-sironnan lisäksi sirota Raman-aktiivisista partikkeleista epäelastisesti. Raman-moodeja on kaksi, joita kutsutaan Stokes- ja anti-Stokes-siirtymiksi. Stokes-siirtymässä systeemi siirtyy perustilalta virtuaalitilan kautta vibraatiotilalle. Siten sironneen fotonin energia on pienempi alkutilanteeseen verrattuna. Anti-Stokes-siirtymässä tapahtuu päinvastoin, jolloin fotonin loppuenergia on alkuperäistä suurempi. Raman-spektroskopiaa voidaan pitää ideaalisena menetelmänä biotieteissä, koska aineen Raman-spektri on ikään kuin sen uniikki sormenjälki.

Nanopartikkelien manipulointi onnistuu esimerkiksi hyödyntämällä dielektroforeesia, jonka teorian *Herbert A. Pohl* esitti jo 1950-luvulla. Ilmiö tarkoittaa neutraalien tai varattujen, polarisoituvien hiukkasten indusoitua liikettä epähomogeenisessa sähkökentässä. Esimerkkinä voi käyttää sähköistä dipolia, joka voi olla pysyvä tai indusoitu. Dipoli asettuu sähkökenttään sen kenttäviivojen mukaisesti. Kentän gradientin takia Coulombin vuorovaikutuksen suuruus dipolin eri päissä poikkeaa toisistaan, mikä johtaa nettovoimaan ja liikkeeseen kentän gradientin mukaisesti. Mikäli partikkelin sähköinen permittiivisyys on väliaineen permittiivisyyttä suurempi, liikkuu se kohti kentän maksimia, jolloin puhutaan positiivisesta dielektroforeesista. Negatiivisesta dielektroforeesista puhutaan vastaavasti silloin, kun väliaineen sähköinen permittiivisyys ylittää partikkelin permittiivisyyden. Silloin partikkeli liikkuu kohti kentän minimiä.

Tässä työssä fluoresoivalla merkkiaine-molekyylillä ja tioli-ryhmällä varustettuja, neljänkymmenen emäsparin pituisia DNA oligonukleotideja vangittiin dielektroforeesin avulla kullasta valmistettujen, sadan nanometrin levyisten elektrodien väliin, jonka jälkeen näytteitä tarkasteltiin konfokaalisilla, laseriin perustuvilla fluoresenssi- ja Raman-mikroskoopeilla. Elektrodikuvio, jossa oli useita elektrodipareja, valmistettiin elektronisuihkulitografialla ja itse elektrodit elektronisuihkuhöyrystimellä. Puolijohdenäytteet tutkittiin pyyhkäisyelektronimikroskoopilla valmistusvirheiden varalta. Fluoresenssimikroskopilla varmistettiin oligonukleotidien vangitsemisen onnistuminen. Raman-spektroskopian tarkoituksena oli tutkia, voisiko sen yhdistää dielektroforeesin kanssa, jolloin lop-

putuloksena voisi olla suhteellisen yksinkertainen, merkkiaineeton, alle mikrometrimittakaavassa toimiva kuvantamismenetelmä, jota voi käyttää lokalisoitujen näytteiden tutkimiseen. Tutkittavien partikkeleiden keräämisellä yhteen pisteeseen, niiden tutkiminen helpottuu, mikäli konsentraatio muuten jäisi alhaiseksi. Samalla voisi yrittää selvittää partikkelien määrää.

Fluoresenssimikroskooppikuvien laatu ei vastannut odotettua, mikä johtui lasereiden heikentyneestä kohdistuksesta. Riittävää Raman-spektriä ei onnistuttu mittaamaan, ainoa signaali saatiin näytteen piialustasta. Mittauksen haasteellisuus tiedettiin ennakkoon, koska käytetyn mikroskoopin spatiaalinen tarkkuus oli ainakin mikrometriluokassa, mutta ei välttämättä sadoissa nanometreissä.

Contents

1 Background and motivation

Nanoscience seems to have almost endless possibilities and it is growing fast as a branch of science. The main element of nanoscience is that it is interdisciplinary. Biology, chemistry and physics all study phenomena that happen in nanoscale. It creates interesting research opportunities and applications that require a vast number of different novel methods and tools to produce and characterize a variety of particles and structures. In many applications it is crucial to position and control single molecules or even atoms in nanoscale.

DNA is a molecule that contains the structural code of a living organism. Due to its role in protein encoding DNA has to be very stable and precisely controllable. DNA has thus proven itself to be useful in various nanoscience applications due to its interesting self-assembly properties [1] [2] [3]. One can for example use DNA molecules as programmed building blocks or scaffolds to organize other molecules [4] [5]. DNA's ability to work as a charge carrier has also been studied [6] [7] [8]. One can also attach different functional modifications to the ends of a DNA molecule.

Molecular modifications are common in bioscience where fluorescence microscopy is used a lot. If a sample is not fluorescent by itself it has to be tagged with a fluorescent dye modification in order to detect it under the confocal microscope. Other types of modifications include different linkers and attachments for instance that can be used to connect particles to each other or to a surface. While molecular modifications are useful and needed they increase the complexity and cost of samples bought from vendors. Because of that it could be beneficial to use some label free imaging technique, for example Raman spectroscopy which is based on Raman scattering rather than fluorescence. Raman spectroscopy can also be regarded as an ideal detection method for bioscience since the Raman spectrum of a molecule is basically its optical fingerprint [9]. The ability to measure both symmetric and non-symmetric chemical bonds effectively in aqueous environments also gives Raman spectroscopy an edge over infrared absorption spectroscopy.

One of the most useful methods to control nanoparticles is to use dielectrophore-

sis (DEP), a phenomenon that causes induced motion of polarizable neutral or charged particles in an inhomogeneous electric field. It was first studied and explained by *Herbert A. Pohl* already in the 1950's and has regained popularity in the nano era [10] [11]. It is a somewhat similar technique to optical tweezers first reported in 1970 by *Arthur Askin* [12] [13].

In this work DNA oligonucleotides with fluorescent dye and thiol modifications were trapped using dielectrophoresis and imaged with confocal and Raman microscopes. Electron beam lithography was used to make the DEP electrodes. The samples were inspected with a scanning electron microscope (SEM) to make sure the quality of the electrodes is sufficient for effective trapping and that there are not any fatal structural defects. Samples with trapped DNA were imaged using a confocal fluorescense microscope to confirm that the trapping setup and parameters work. The goal of the Raman spectroscopy was to see if it could be combined with dielecrophoresis to create a very precise and label free imaging technique that could be utilized in bioscience and potentially reach submicron resolution. If for example there were Raman active nano-objectives in a sample but the concentration was rather low it would be beneficial to gather them to a single point in order to detect them more easily. That way one could also try to make a rough estimate of the particle count or concentration.

2 Theoretical background

2.1 General insights

The three aspects of this work are nanofabrication, particle manipulation and imaging. Some of the methods utilize equipment available commercially and others rely on in-house tools. Nanofabrication in this case involves electron beam lithography, reactive ion etching and ultra high vacuum evaporation of metals. Particle manipulation is carried out by dielectrophoretic trapping of DNA oligonucleotides using an in-house trapping setup. Imaging of the oligonucleotides is based on fluorescence and Raman scattering while the working principle of the scanning electron microscope used for electrode inspection relies on

interactions between electrons and matter. Theoretical background and working principles of these methods and techniques are presented in this section. In addition to that more specific details regarding this work are given.

2.2 Deoxyribonucleic acid

2.2.1 Basic structure

Deoxyribonucleic acid (DNA) is one of the ribonucleic acids the other being ribonucleic acid (RNA). The structure of DNA consists of a polymeric chain and four different bases attached to that backbone. The repeating unit of the chain is formed by connecting the hydroxyl group on the 5′ carbon atom of a 2′-deoxyribose monomer to a phosphate residue. The 3′ hydroxyl of the same monomer is again connected to another phosphate residue forming the polymer chain [14, p. 92]. One base is connected to each monomer. The four different basic groups are adenine, guanine, thymine and cytosine. The repeating unit of the polymer connected to a base is called a nucleotide. Adenine can form a hydrogen bond with thymine as guanine can pair with cytosine leading to the famous double helix secondary structure of the DNA molecule. DNA can also exist in other forms such as single stranded for example. In that case the notation ssDNA can be used to specify the form. Double stranded DNA is in a similar manner called dsDNA. The basic structure of DNA is illustrated in figure 1.

2.2.2 Oligonucleotides

The polymers consisting of different nucleotides are called polynucleotides. Oligonucleotides (oligos) are short polynucleotides that normally have the length of a few tens of base pairs (*bp*) or less. One *bp* is roughly 3.4 Å long. [16, p. 566-567] Although the length is measured in base *pairs* oligonucleotides are always single stranded by definition [17, p. 143]. Various modifications are often attached to the 3′ and 5′ ends of the oligonucleotides. They include different reporter groups such as fluorophores and biotin, and linkers such as amino, thiol and carboxylate groups [17, p. 159].

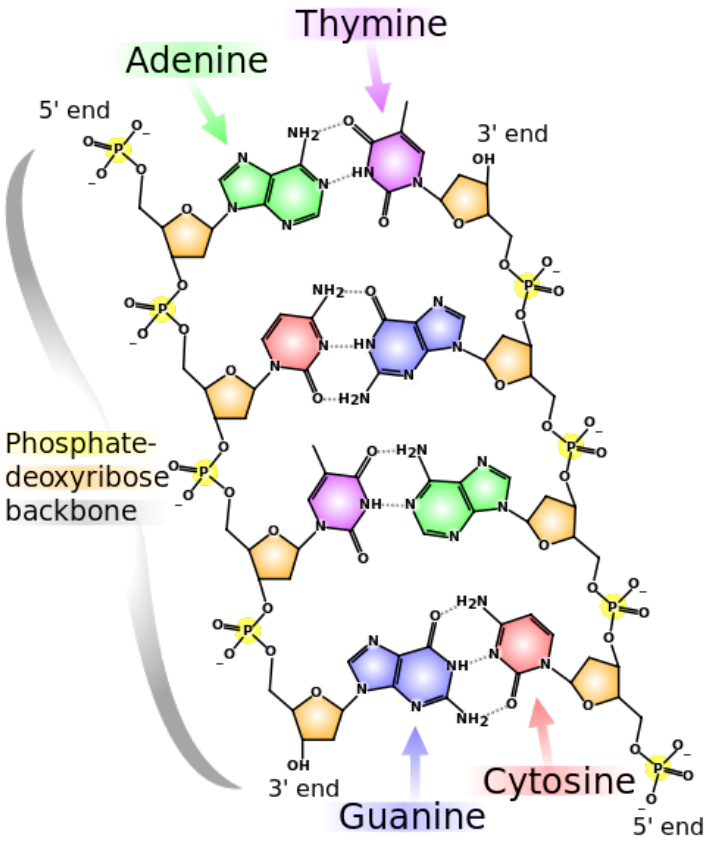

Figure 1: The basic chemical structure of DNA. Two strands are linked together with hyndrogen bonds shown as dotted lines forming the double-helix structure. In the image the sugar-phosphate backbones with all the four bases marked with different colours and the 3′ and 5′ ends can be seen. [15]

2.3 Dielectrophoresis

Dielectrophoresis is a phenomenon that causes induced motion of polarizable neutral or charged particles in an inhomogeneous electric field [11]. An example of a polarizable particle is an electric dipole that can either be permanent or induced. The charge separation of the dipole aligns it along the electric field. Because the field is inhomogeneous the electric force acting on the ends of the dipole will differ resulting in a net force that causes its motion. The basic principle of the dielectrophoretic force is shown in figure 2. In an inhomogenous

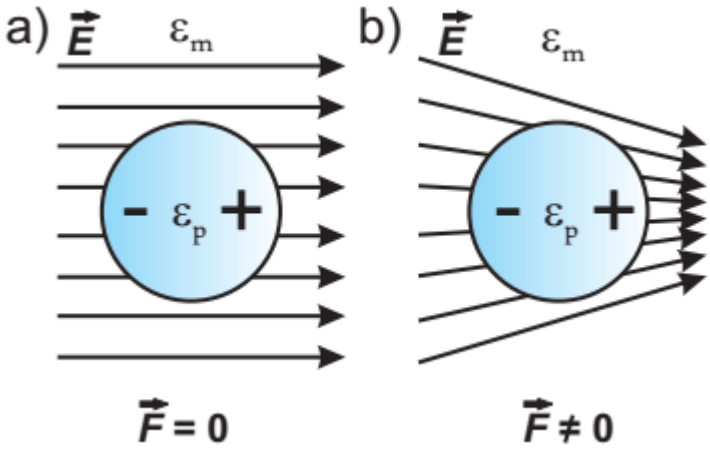

Figure 2: The basic principle of the DEP force is shown here. a) A polarized particle in a homogeneous electric field. The forces acting on the sides of the particle cancel each other out. No movement occurs. b) The field is inhomogeneous and thus the net force is nonzero resulting in movement. ε_p and ε_m are the relative permittivities of the particle and the medium, respectively. [18]

electric field the translational force on a dipole is [19, p. 189]

$$\vec{F} = (\vec{\mu} \cdot \nabla)\vec{E} \tag{1}$$

where $\vec{\mu}$ is the dipole moment and $\vec{E}$ the electric field acting on the dipole. Due to an induced polarization of a particle having isotropic, homogene and linear polarizability we can write

$$\vec{\mu} = \alpha V \vec{E} \tag{2}$$

where α is the polarizability per unit volume and V the volume of the particle. Inserting equation (2) into (1) will give

$$\begin{aligned} \vec{F} &= \alpha V (\vec{E} \cdot \nabla)\vec{E} \\ &= \frac{\alpha V}{2} \nabla |\vec{E}|^2 \end{aligned} \tag{3}$$

For a spherical particle in a medium the internal electric field can be written as

$$\vec{E}_\mathrm{int} = \frac{3\varepsilon_\mathrm{m}}{\varepsilon_\mathrm{p} + 2\varepsilon_\mathrm{m}} \tag{4}$$

where ε_{p} and ε_{m} are the relative permittivities of the particle and the medium, respectively. The induced polarization per unit volume for the particle is

$$\vec{P} = \varepsilon_0(\varepsilon_{\mathrm{p}} - \varepsilon_{\mathrm{m}})\vec{E}_{\mathrm{int}} \tag{5}$$

Equation (2) can now be rewritten as

$$\vec{\mu} = V\vec{P} = \alpha V\vec{E} \tag{6}$$

Using equations (4) and (6) α can be defined as

$$\begin{aligned} \alpha &= \frac{|\vec{P}|}{|\vec{E}|} \\ &= \varepsilon_0(\varepsilon_{\mathrm{p}} - \varepsilon_{\mathrm{m}})\frac{|\vec{E}_{\mathrm{int}}|}{|\vec{E}|} \\ &= \frac{3\varepsilon_0\varepsilon_{\mathrm{m}}(\varepsilon_{\mathrm{p}} - \varepsilon_{\mathrm{m}})}{\varepsilon_{\mathrm{p}} + 2\varepsilon_{\mathrm{m}}} \end{aligned} \tag{7}$$

Inserting equation (7) to equation (3) will give the dielectrophoretic force acting on a spherical particle.

$$\vec{F} = 2\pi r^3\varepsilon_0\varepsilon_{\mathrm{m}}\left(\frac{\varepsilon_{\mathrm{p}} - \varepsilon_{\mathrm{m}}}{\varepsilon_{\mathrm{p}} + 2\varepsilon_{\mathrm{m}}}\right)\nabla|\vec{E}|^2 \tag{8}$$

where r is the radius of the sphere. A part of the equation (8) can be rewritten as the Clausius-Mossotti factor K [20, p. 36]

$$K = \frac{\varepsilon_{\mathrm{p}} - \varepsilon_{\mathrm{m}}}{\varepsilon_{\mathrm{p}} + 2\varepsilon_{\mathrm{m}}} \tag{9}$$

From equation (9) can be seen that when $\varepsilon_{\mathrm{p}} > \varepsilon_{\mathrm{m}}$ particles are attracted towards the higher field intensity and when $\varepsilon_{\mathrm{p}} < \varepsilon_{\mathrm{m}}$ they are attracted towards the lower field intensity. These cases are thus called *positive dielectrophoresis* and *negative dielectrophoresis* respectively [20, p. 37].

In the case of complex relative permittivities equation (8) should be given the

form [21]

$$\vec{F} = 2\pi r^3 \mathrm{Re}[\varepsilon_0 \varepsilon_\mathrm{m}^* \left(\frac{\varepsilon_\mathrm{p} - \varepsilon_\mathrm{m}}{\varepsilon_\mathrm{p} + 2\varepsilon_\mathrm{m}} \right)] \nabla |\vec{E}|^2 \tag{10}$$

Relative permittivities are now defined as

$$\varepsilon_\mathrm{p} = \varepsilon'_\mathrm{p} - \varepsilon''_\mathrm{p} = \varepsilon'_\mathrm{p} - \mathrm{j}\frac{\sigma'_\mathrm{p}}{\omega} \tag{11}$$

and

$$\varepsilon_\mathrm{m} = \varepsilon'_\mathrm{m} - \varepsilon''_\mathrm{m} = \varepsilon'_\mathrm{m} - \mathrm{j}\frac{\sigma'_\mathrm{m}}{\omega} \tag{12}$$

where ε'_p and ε'_m are the in-phase permittivities of the particle and the medium respectively, ε''_p and ε''_m are the out-of-phase permittivities, σ'_p and σ'_m are the in-phase conductivities and ω is the angular frequency.

Trapping particles involves also another force which is the thermal drag force. For a spherical particle it can be approximated as [22]

$$F = \frac{k_B T}{2r} \tag{13}$$

DNA however is quite far from spherical. Therefore it is better to use the concept of Brownian motion and its thermal energy

$$U_{Th} = \frac{3}{2} k_B T \tag{14}$$

One can also define a DEP potential, so that the gradient of it yields the DEP force. The DEP potential is thus

$$U_{DEP} = -\frac{1}{2} \alpha' E^2 \tag{15}$$

where α' is the total polarizability of the trapped object. Combining equations (14) and (15) gives the total potential energy

$$U_{tot} = U_{Th} + U_{DEP} = \frac{3}{2} k_B T - \frac{1}{2} \alpha' E^2 \tag{16}$$

This equation dictates if a particle can be trapped or not. When the total poten-

tial energy remains positive Brownian motion outweighs the dielectrophoretic force and the particles will not be trapped. Respectively when the DEP potential is greater than or equal to the thermal potential the particles are trapped in the potential well induced by the dielectrophoretic force. The DEP potential is illustrated in figure 3 in the case of nanoscale fingertip like electrodes with voltage applied across them.

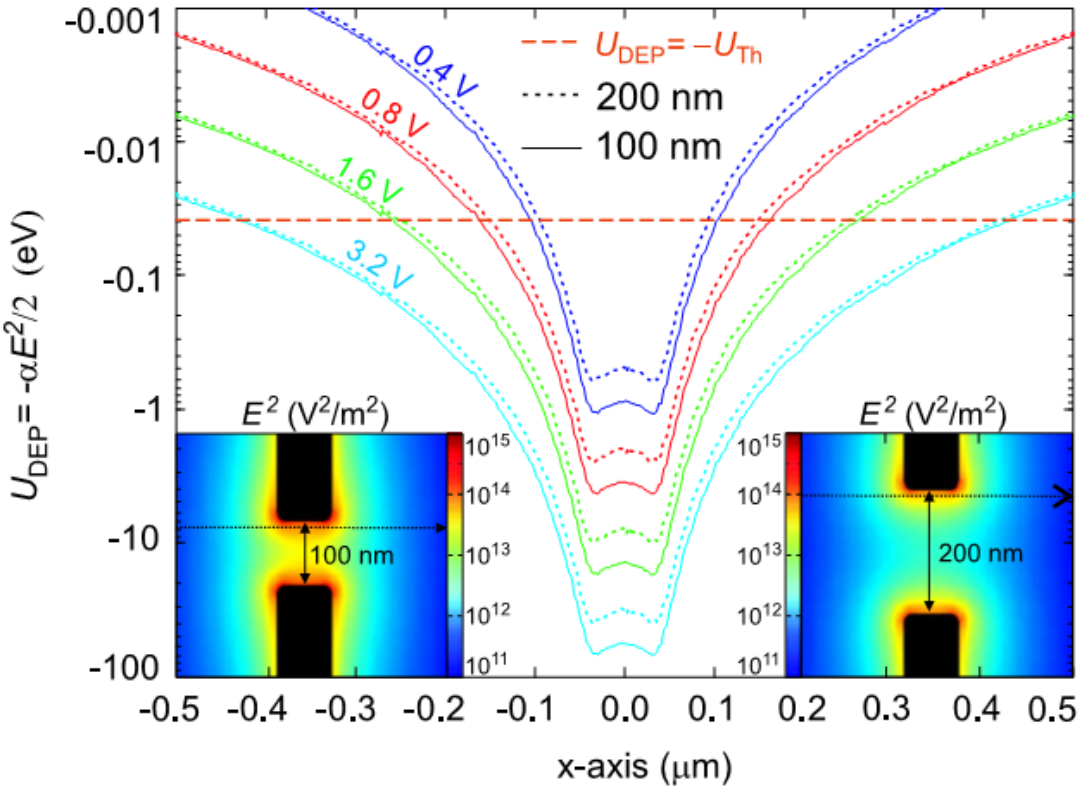

Figure 3: The DEP potential as a function of the perpendicular distance from the tip of the electrodes following the dotted line depicted in the insets. The four potentials represent scenarios with different trapping voltages. The horizontal dotted line represents the situation where the DEP potential and the thermal energy are equal. [22]

2.3.1 Dielectrophoretic trapping of DNA

DNA is commonly trapped using metallic fingertip electrodes [6][22][23][24][25] but electrodeless techniques [26] and carbon nanotube electrodes [27] have also

been studied. Gold is a commonly chosen material for electrodes because of its bonding with thiol [28]. DNA molecules modified with thiol linkers can thus be immobilized to gold electrodes for further study. Size of the DNA molecules, the gap length between the electrodes, medium and the voltage and the frequency of the signal generator all affect the trapping.

When the size of the DNA decreases its polarizability decreases also [22]. Thus one has to increase the electric field to successfully trap smaller DNA. However polarizability per base pair increases as the size of the DNA decreases. Frequency does not have a very significant role in the trapping process. Lower frequencies lead to higher yields but locality is better with higher frequencies. A good compromise of yield and accuracy is $\sim 1\ \mathrm{MHz}$.

2.4 Scanning Electron Microscopy and Electron Beam Lithography

2.4.1 Scanning Electron Microscopy

Electron microscopes are used in imaging of micro- and nanoscale objects such as viruses or semiconductor components. Wavelength of an electron beam can be calculated using the *de Broglie* relation [29, p. 1494]

$$\lambda = \frac{h}{p} = \frac{h}{\sqrt{2meV}} \tag{17}$$

where h is the Planck's constant, p the momentum of the electron beam, m the mass of the electron, e the elementary charge and V the acceleration voltage. If we now assume an acceleration voltage of $40\ \mathrm{kV}$ the wavelength will be roughly $6\ \mathrm{pm}$. As a comparison the wavelength of visible light is between $400\ \mathrm{nm}$ and $700\ \mathrm{nm}$ which is higher by five orders of magnitude. This means that the diffraction limit will not pose a problem when imaging small nanostructures using an electron microscope as it would with a conventional optical one. Due to their short wavelength electron beams are also used in pattern generation technique known as electron beam lithography. Resolution of this technique is limited by the utilized resist and is somewhere between $5\ \mathrm{nm}$ and $10\ \mathrm{nm}$ depending on the level of equipment. As a comparison the most advanced photolithography processes currently use a process node of $14\ \mathrm{nm}$. It may not be strictly the true

linewidth of the process but gives a good estimate of it. $14\ \mathrm{nm}$ is for example used in the lithography process of *Broadwell* microprocessors developed by *Intel* [30].

2.4.2 Electron Gun

Electron beam is generated with an electron gun which uses thermionic or field emission to create free electrons. In thermionic emission the cathode is heated to a point where electrons overcome the work function of the cathode material and are then accelerated towards the anode. Tungsten and lanthanum hexaboride $\mathrm{LaB_6}$ are consider good materials for thermionic emission because of their low work function and high melting point. Tungsten cathodes are usually hairpin shaped while $\mathrm{LaB_6}$ rods use a sharp tip in order to achieve point-like emission area. Field emission guns use an electric field strong enough to alter the potential barrier at the emission point that electrons can tunnel through it even at room temperature. With field emission two anodes are needed. The first one generates the field affecting the potential barrier and the second is used for accelerating the electrons to their final energy as in thermionic emission. Acceleration voltages can vary from a few hudred volts to tens of kilo volts. The anode also works as a collimator for the beam. [31, p. 23–25] [32, p. 13–18]

2.4.3 Magnetic Lenses

After the anode the electron beam is focused using magnetic lenses. A typical lens consists of a solenoid magnet since it creates an axial magnetic field with rotational symmetry. The lens focuses electrons of the same kinetic energy to the same focal point. The lens system of a SEM usually consists of two condenser lenses and a final focusing lens. Scanning coils which are used to position the electron beam spot are located before the last lens. [32, p. 1, 20] [31, p. 26]

2.4.4 Detection

The studied sample is attached to a stage which may be tiltable. The stage is grounded since the sample must not accumulate electric charge during imaging.

Therefore at least the surface of the sample must be conductive. Scanning electron microscope works in a way that a sample being imaged is scanned pixel by pixel by a point-like focused electron beam. Electrons interacting with the sample are detected using different methods and the signals are then combined to create an image. Most of the electrons are backscattered from the sample while the rest either travel through or get absorbed by it. Primary electrons interacting with the target create secondary electrons when they hit low energy level electrons in the sample atoms and release them. Vacancies are filled with electrons from upper electron shells creating x-rays. If an x-ray photon hits an electron on a higher electron shell it may also release it. Electrons created this way are called Auger electrons. Cathodoluminescence is also possible when the electron beam causes electrons to move from the valence band to the conduction band creating an electron hole pair. Photon may be emitted when the electron hole pair recombinates. [33, p. 31–32] [31, p. 2, 10, 22]

Backscattering electrons are detected above the sample. Since every electron can not be detected using this detector shadows are introduced to the image. Backscattered electrons give information about the composition of the surface of the sample. Due to high energy they also travel to the detector from deeper depths of the sample. Secondary electrons however have low energy and can only be detected at close proximity of the surface. They give information about the surface topography. Secondary electrons are collected to a dedicated detector using a bias voltage which is selected so that backscattered electrons are not collected but most of the secondary electrons are. Auger electrons and x-ray photons are used to inspect the elemental composition of the studied sample. [31, p. 3, 27–29]

2.4.5 Adjustable Parameters

Strengths of the SEM are high resolution, high contrast and high depth of field while its weaknesses include charging, aberrations, astigmatism, sensitivity to vibrations and other external factors. The system also has to be in a vacuum. High resolution can be achieved using a high acceleration voltage. A voltage too high can however cause physical damage to the sample. A current too high

causes charging, which can be controlled by apertures. High contrast requires small diffusion area of secondary electrons. The diffusion area becomes larger at higher acceleration voltage which lowers the contrast. High depth of field means (DoF) that the image is focused far around the focal point of the system. This requires the electron beam to be as narrow as possible as far as possible. Since the beam spot can be close to $1\ \mathrm{nm}$ a high DoF is possible. Large working distance and small aperture maximise the DoF while making the images grainy. [34, p. 5, 18]

Charging inhibits normal creation of secondary electrons leading to unusual contrast and deformation of the image. The effect can be countered by lowering the acceleration voltage or the intensity of the electron beam. Coating the sample with a thin metal layer also an option. The electron lens system introduces aberrations to the image like optical lenses do. Spherical aberrations occur when the lens focuses parallel rays to different points on the optical axis. Chromatic aberration emerges when the electron beam is not fully monochromatic in energy. The lens system then refracts different energy electrons to different focal points. Astigmatism blurs images due to nonidealities of components of the lens system. It can be countered using stigmator lenses. Vibrations and external magnetic fields cause image distortion and jagged edges due to unusual eletron propagation and sample movement. Low vacuum levels cause problems when electrons scatter from the particles in the chamber. [31, p. 18] [34, p. 14, 18, 20] [32, p. 23]

2.4.6 Electron Beam Lithography

The first step of the lithography process is creating a CAD-file containing the desired pattern and loading it to he memory of the beam writer. In the cleanroom the sample substrate is prepared and cleansed thoroughly and a resist layer is spinned on top of it and then baked. The resist is the layer that reacts chemically with the electron beam. It has three components: the reactive polymer, its carrier matrix and solvent. A resist type commonly used with electron beam lithography is Poly(methyl methacrylate) (PMMA). There are two types of resists: positive and negative. When using a positive resist areas exposed to

electrons are dissolved during the developement of the resist. Electrons break the polymers making then more soluble. Negative resist works the opposite. Exposure to electrons induces crosslinking of the polymer chains which make them insoluble in the developer chemical. The resist also protects the substrate. A pipet can be used to apply the resist layer on top of the substrate. The sample is then put to a spinner that flattens the layer and removes the excessive amount of resist applied. After that the resist is baked which hardens it while evaporating its solvent. Depending on applicationa a mono or multilayer resist can be used. [35, p. 93, 103–104, 107]

The process step that creates the wanted pattern on the resist is called exposure. The pattern is generated pixel by pixel scanning the resist layer with an electron beam. First the electron beam is focused, parameters including beam intensity and acceleration voltage are chosen and starting point is set. The beam intensity and energy affect its spreading in the resist and efficiency of the exposure. Resist sensitivity describes the dose the resist absorbs when hit by the electron beam. Unit of the dose is $\mathrm{As/cm^2}$. The dose has a great impact on the success of the exposure and its optimal value depends on the resist and the developer chemical. The smallest achievable linewidth using electron beam lithography is in the order of a few nanometres. Most of the exposure is due to secondary electrons. The limiting factors are the size of the electron source, lens aberrations and spreading of the collimated beam. Using a too intense beam causes Coulomb repulsion due to charging. Electrons also scatter in the resist layer widening the exposed area making it larger than the beam spot. Thinner resist layer causes less scattering than a thick one but can cause other issues. A thin layer does not withstand etching as well and is more prone to structural defects. The exposure process is slow compared to photolithography that allows the pattern to be exposed in one single flash of light. Electron beam lithography is also a maskless technique on the contrary to the photolithography that needs a photomask. While photolithography is a fast parallel process that is suited for IC industry, electron beam lithography is a slow serial process used mainly in research where large number of samples are not needed. The upside of electron beam lithography is the lower theoretical linewidth limit compared

to photolithography. [35, p. 93, 95] [36, p. 12–14] [37, p. 11, 20, 28]

After the exposure the resist is developed. The sample is emerged in in a chemical that dissolves either the exposed or unexposed areas of the resist depending on the type of the resist. If a multilayer resist has been used an 'undercut' profile is created. If the top layer is thinner electrons scatter less in it making it underexposed compared to the bottom layer resulting in a wider cavity in the bottom layer. The undercut profile can make the lift-off process easier after growing a thin film on the substrate. After the developement resist residues can be cleaned using reactive ion etching. [36, p. 15]

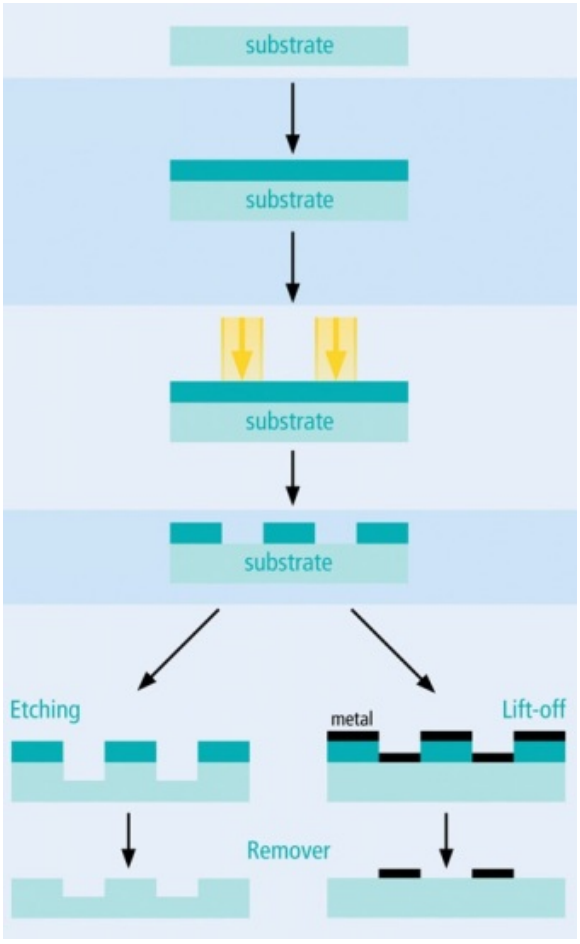

Figure 4: Process steps of electron beam lithography. Starting from the top: plain substrate, spin coating of the resist, exposure, developing, etching (left) and deposition of metal thin film (right), lift-off. [38]

Developed samples can undergo various steps to grow thin films on them or to be etched. One common example is growing a metal thin film using physical vapor deposition (PVD). The final step is the lift-off process. The sample is emerged in acetone that dissolves the resist completely along with the deposited material on top of it. Since PVD has poor step coverage the thin film should be discontinuous at the edges of the resist meaning the evaporated pattern should stay intact. However if the resist layer is too thin there may be enough material deposited on its sidewalls to form a continuous film reaching from the top of the resist to the substrate. The thin film may then suffer damage rendering the sample useless when it breaks in the lift-off. [35, p. 288–289] Process steps of the electron beam lithography are depicted in figure 4.

2.5 Fluorescence Microscopy

2.5.1 Confocal Scanning Laser Microscope

The basic components of a confocal scanning laser microscope (CSLM) are point illumination and detection systems, a confocal lens system and an image scanning system. The emitted laser beam goes through a pinhole to a beam expander. The expanded beam is then focused to a point on the studied sample by the objective lens of the system. The scattered light is reflected back to the objective lens and deflected by a beamsplitter through another pinhole to a detector. The sample stage is raster scanned to form an image point by point. [39, p. 68–69]

Lasers are used as an illumination source because of their characteristics. Lasers provide a bright light source that emit coherent single-frequency light. That way the optical filtering system can be simplified which is important if the system is used in fluorescent imaging because of the separation of the exciting and fluorescent light. High brightness is needed because the quantum yield of fluorescent dye molecules is usually poor. The mode structure of the laser is also important. TEM_{00} mode is used because of its uniform intensity distribution. Therefore theoretically no pinhole as a spatial filter is required because the laser is seen as a point source at infinity. Since the beam spot cannot be ideal in reality

pinholes are used to filter out the edges of the beam spot. The intensity stability and pointing stability are the two most important specifications of the laser since changes in the intensity or the pointing direction of the source directly alter the intensity of the scattered light from the sample. If no pinhole is used the pointing instability can change the position of the beam spot on the sample. Wavelength stability is usually less important since small changes in the source wavelength affect the image only slightly in most applications. $\mathrm{He-Ne}$ and Ar^+ gas lasers and diode lasers are commonly used in CSLMs because they are inexpensive, reliable and provide a wide selection of wavelengths. Ar^+ lasers are used especially for fluorescent imaging because of their blue and green emission lines. The illumination system should also include a magnification system to ensure the beam to fill the objective lens uniformly. Otherwise the effective numerical aperture of the lens is reduced and its depth response is broadened because of the decreased light intensity near the edges of the lens. The expanded beam can be for example five to ten times larger than the objective lens to overcome this problem. The focusing system is usually a combined pinhole beam expander. [39, p. 69–71]

The objective lens is the most important component of a CSLM. Therefore it is extremely important that the optical quality of the lens is the highest possible. Spherical and axial chromatic aberrations of the lens system are the most common factors that affect the resolution a confocal scanning optical microscope. The effect is increased because both the incident and the light scattered from the sample use the same objective lens. Spherical aberration can be reduced by using high-quality lenses. Chromatic aberration is minimized by lens design. In the CSLM the objective lens is infinity corrected. Aberrations are therefore minimized for an infinite tube length which means plane waves from a point source at infinity are focused onto the sample. Most of the infinite tube length lenses but not all are dry lenses that are designed to be used without immersion fluids. [39, p. 71–72]

Scanning the stage while using the objective stationary on axis reduces aberrations compared to a case where the beam is scanned. In order to achieve a stage resolution of for example $100\ \mathrm{nm}$ or better, high accuracy and vibration stability

is required. In addition to accurately measuring the horizontal stage position and feeding it to the control electronics the precise vertical separation of the sample and the objective lens is critical to ensure successful imaging. The distance has to be within depth of focus of the microscope. Piezoelectric elements are commonly used due their fast operation rigidity. [39, p. 73]

Quality of the intermediate optics such as the beam splitter is not as important as the quality of the objective lens. For a $\frac{50}{50}$ beamsplitter an error of $\frac{\lambda}{4}$ single pass of the transmitted wavefront is usually good enough. The point detector can block any ghost reflections coming from the bottom surface of the beamsplitter if it is thick enough. The pinhole lens in front of the detector benefits from a relatively long focal length. That way a larger detector pinhole can be used which makes it easier to be aligned properly. However while a larger pinhole transmits more light and gives a stronger signal to the detector it also decreases resolution. Smaller pinhole has better resolution but worse signal-to-noise-ratio. Thus the optimal solution depends on the sample. A pinhole with a diameter of the half-power width of the Airy pattern of the pinhole lens is commonly a good choice. [39, p. 74]

The detector is essentially a photodiode. An optical filter can be used with it to prevent ambient light from hitting it. The generated electric signal is amplified and combined with the positional signals from the sample stage electronics to produce an image. [39, p. 74–75]

2.5.2 Fluorescence Imaging Mode

The strength of the CSLM compared to the traditional optical microscope is its ability to omit the possible fluorescent glare coming from the out-of-focus planes in the sample. It allows one to see much more detailed images of the sample. The two main limitations of fluorescent imaging with the CSLM in terms of detail are the bleaching of the fluorophores and the performance of the light collecting system. Lasing power of only more than a few milliwats can bleach most fluorophores so care must be taken. The collection efficiency of the fluorescent light can be as low as 0.2% in a CSLM. The finite solid angle of the objective lens,

reflection losses in the optical system, the pinhole and the efficiency of the detector all contribute to this. High numerical aperture lenses and a large separation of excitation and fluorescent wavelengths ensure the efficiency is sufficient for imaging. [39, p. 311, 313–314]

Due to the ability to omit light coming from the out-of-focus planes three-dimensional imaging is possible. It allows morphological analysis of the sample without being invasive meaning that its structures and functionality are preserved. A technique called optical sectioning is used to aquire two-dimensional images of the sample that are used to reconstruct its three-dimensional shape. The fine z-stepping (image assumed to be on the x-y plane) is done by moving either the sample stage or the objective lens. Three-dimensional information can be useful when imaging cells for example. [40, p. 435-437]

2.5.3 Fluorescent Labels

Fluorescence imaging is especially useful in life sciences where interactions between biomolecules and different ionic and molecular species are studied. In order to observe these interactions the particles in question have to be marked with fluorescent labels. Resolution of this technique is on a nanometre scale and its sensitivity can reach a single-molecule level. Adjustable parameters include the intensity, lifetime and anisotropy of the fluorescent emission and as well the shape of the excitation and emission spectra. [41]

A suitable label should be easily excitable without exciting the rest of the system simultaneously, detectable with conventional equipment and have a high molar absorption coefficient at excitation wavelength and a high fluorescence quantum yield. The label should also be soluble in buffers, body fluids and cell culture media while staying sufficiently stable in aforementioned environments and conditions related to them. Functional groups for site-specific labeling, well-known photophysical properties and reproducible quality are also required. In addition to these attributes there are specific application related requirements. Organic dye molecules have traditionally been used as fluorescent labels since they are very versatile. Inorganic quantum dots (QDs) however

have emerged to compete with them [42]. II/VI and III/V semiconductor crystals are the most used QDs in bioanalytics and medical diagnostics although some of them are cytotoxic precluding their use in *in vivo* applications. [41]

The optical properties of organic dyes depend on their electronic transitions. There are typically two different origins of the emission. One is from an optical transition delocalized over the whole molecule and the second is from intramolecular charge transfer transitions. Because of the resonant nature of the first type, dyes utilizing it are called resonant dyes. Dyes of the second type are called CT dyes respectively. Most cyanines for example are resonant dyes with slightly structured, comparatively narrow and often mirrored absorption and emission bands. They also have a small polarity-insensitive Stokes shift, high molar absorption coefficients and moderate-to-high fluorescence quantum yields. Stokes shift is the difference between the spectral positions of the maxima of the longest wavelength absorption and the fluorescence arising from the same electronic transition. Organic dyes in general have high quantum yields in the visible light range and moderate yields in the near infrared region. The fluorescence lifetimes of organic dyes in those wavelength regions are usually around $5\ \mathrm{ns}$ and $1\ \mathrm{ns}$ respectively. [41]

Labels are bound to the biomolecules covalently or attached noncovalently via suitable functional groups. A large variety of different functionalized dyes is available commercially. Labeling protocols, purification and characterization tehniques and information of the site-specificity of the labeling are all well known. Site-specificity can still be difficult to achieve, and high label densities can cause fluorescence quenching depending on dye structure, charge and hydrophilicity. [41]

The label microenvironment and temperature affect the spectroscopic properties of the dyes. The spectral position, the fluorescence lifetime and the intensity of absorption and emission bands of the organic dyes can change because of that. Features of the microenvironment include its hydrogen bonding ability, viscosity, pH and ionic strength, possible surfactants, fluorescence quenchers and conjugated molecules. Spectral characteristics of resonant dyes such as cyanines are commonly only moderately affected by these changes.

However their fluorescence quantum yield and lifetime can change more than that, and aggregation-induced fluorescence quenching can be possible. [41]

Semiconductor nanocrystals have a narrow, tunable and symmetric emission spectrum compared to organic dye molecules. They are also photochemically more stable than organic dyes. Nanocrystals are in general complementary, and in some cases superior to organic dyes. The narrow excitation spectrum and broad emission spectrum of organic dyes makes simultaneous excitation of different dyes difficult and introduces crosstalk between detection channels. Therefore quantification of the relative amounts of diffrent labels becomes difficult. Ideally multicolor experiment labels should have a narrow and symmetric emission spectrum with spectrally resolvable energies. Every label should also be excitable with a single wavelength. Nanocrystal labels could provide a solution to this since they can be efficiently excited at any shorter wavelength than the main absorption peak while retaining the same narrow and symmetric emission spectrum. Variation of the size and the material alters the emission and excitation peaks of the nanocrystal. Decreasing size leads to shorter wavelength. Emission peak range from $400\ \mathrm{nm}$ to $2\ \mu\mathrm{m}$ with a FWHM of $20\ \mathrm{nm}$ to $30\ \mathrm{nm}$ can be achieved. Nanocrystal labels consist of a core and a surface layer. The excitation is confined to the core preventing photochemical degradation and eliminating nonradiative relaxation pathways. The surface is designed to interact with the sample through electrostatic interactions and hydrogen-bonding or ligand-reseptor interaction. [42]

2.6 Raman Spectroscopy

2.6.1 Basic Principles

Raman spectroscopy is based on a phenomenom called *Raman scattering* discovered in the 1920s by Indian physicists *C. V. Raman* and *K. S. Krishnan* [43]. It is one of the two possible types of light scattering the other being *Rayleigh scattering*. Using classical theory we can write [44, p. 15–16]

$$|\vec{E}| = E_0 \cos(2\pi\nu_0 t) \tag{18}$$

where E_0 is the vibrational amplitude and ν_0 is the frequency of the incident light (eg. a laser) and t is the time. Using equation (7) we can now write

$$|\vec{P}| = \alpha E_0 \cos(2\pi\nu_0 t) \tag{19}$$

Nuclear displacement q of a molecule can be written as

$$q = q_0 \cos(2\pi\nu_m t) \tag{20}$$

where q_0 is the amplitube of the vibration and ν_m the vibrational frequency of the molecule. If a small amplitude of vibration is assumed α is a linear function of q and therefore

$$\alpha = \alpha_0 + \left(\frac{\partial\alpha}{\partial q}\right)_0 q + \dots \tag{21}$$

where α_0 is the polarizability of the molecule at the equilibrium position and $\left(\frac{\partial\alpha}{\partial q}\right)_0$ is the rate of change of α as a function of q at the equilibrium position. Using equations (19), (20), (21) and a trigonometric identity the electric dipole moment can be written as

$$\begin{aligned} |\vec{P}| &= \alpha_0 E_0 \cos(2\pi\nu_0 t) + \left(\frac{\partial\alpha}{\partial q}\right)_0 q E_0 \cos(2\pi\nu_0 t) \\ &= \alpha_0 E_0 \cos(2\pi\nu_0 t) + \left(\frac{\partial\alpha}{\partial q}\right)_0 q_0 E_0 \cos(2\pi\nu_0 t)\cos(2\pi\nu_m t) \\ &= \alpha_0 E_0 \cos(2\pi\nu_0 t) + \frac{1}{2} q_0 E_0 [\cos(2\pi(\nu_0+\nu_m)t) + \cos(2\pi(\nu_0-\nu_m)t)] \end{aligned} \tag{22}$$

The first term of the equation (22) stands for the Rayleigh scattering of light from the vibrating molecule (an oscillating dipole with a frequency ν_0) and the second term represents the Raman scattering. There are two different modes for Raman scattering called the *Stokes* $\nu_0-\nu_m$ and *anti-Stokes* $\nu_0+\nu_m$ lines. It is important to note that $\left(\frac{\partial\alpha}{\partial q}\right)_0$ must be nonzero in order for the molecule to be Raman-active. The energy levels of Raman scattering are illustrated and compared to the ones of Rayleigh scattering and infrared absorption in figure 5. Since Rayleigh scattering is elastic the molecule returns to its initial state after the scattering event. Raman scattering is inelastic which means there is a frequency shift between

the incident and the scattered light. Stokes lines represent the case where the final state of the molecule is a vibrational energy state above its ground state. Anti-Stokes lines represent the opposite. The virtual energy states seen in figure 5 are not real excited states since these are scattering events and absorption and emission processes are not involved. As stated by the *Maxwell-Boltzmann distribution law* the population of the molecules at the ground state is significantly larger than at any vibrational state [44, p. 12]. Therefore the Stokes lines are stronger than the anti-Stokes lines. Since they give the same information as the anti-Stokes lines it is common to measure only the Stokes lines. The intensity of the Raman scattering is still very weak, only $\sim 10^{-5}$ of the incident light. [44, p. 15–16]

2.6.2 Instrumentation

The basic components of a Raman microscope are an excitation source, sample illumination and collection system, wavelength selector and a detection and computer control/processing systems. The excitation source is usually a continuous-wave (CW) laser [44, p. 95]. Lasers are used because they produce highly monochromatic and coherent light. Monochromaticity of a laser is presented by its spectral line width $\Delta\lambda$, the lower the better. Relative line width $\Delta\lambda/\lambda$ is commonly used when measuring the monocromaticity. $\mathrm{He\text{-}Ne}$ laser for example has a relative line width of $\sim 10^{-11}$ to $\sim 10^{-13}$. Coherency means coherency both in time and space. Time coherency is only meaningful for pulsed lasers. It corresponds to a case when the two laser beams emitted from the same source at the same time are superposed to the same point. Space coherency presents a case when the beams emitted from the same source at different times are superposed to the same point. The coherence time τ_c and coherence length L_c of a $\mathrm{He-Ne}$ laser can be $1.3 \cdot 10^{-4}$ s and $4 \cdot 10^{6}$ cm. Laser beams also achieve high brightness and a high degree of polarization while being extremely directional. The brightness of a laser beam at its focal point can exceed the brightness of the Sun by a factor of $\sim 10^{6}$. For a single-mode $\mathrm{He-Ne}$ laser the solid angle $\Delta\Omega$ measuring the directionality can be as low as 10^{-6} radian. [46, p. 56–57]

Typical CW gas lasers used besides the $\mathrm{He-Ne}$ (632.8 nm) include $\mathrm{Ar^+}$ (351.1 nm

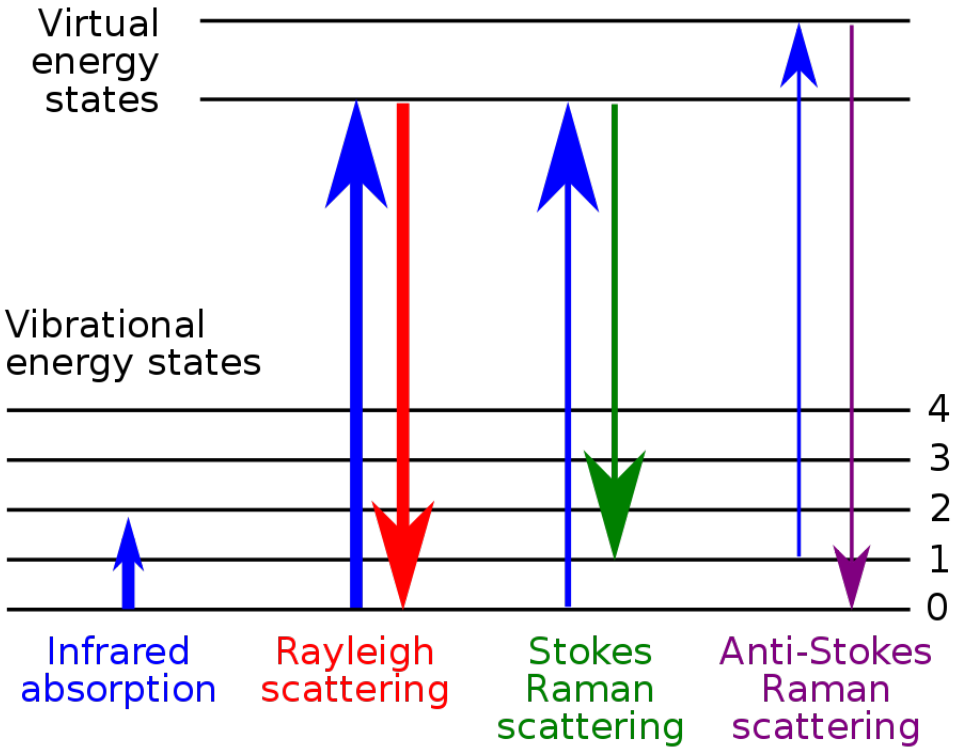

Figure 5: Energy levels of Raman scattering and infrared absorption and Rayleigh scattering as comparison. From left to right: infrared absorption from the ground state to a vibrational state, elastic scattering of the incident photon known as Rayleigh scattering, Stokes shift resulting in the molecule going from the ground state to a vibrational state, anti-Stokes shift resulting in the molecule returning to ground state from a vibrational state. [45]

to $514.5\ \mathrm{nm}$) and Kr^+ ($337.4\ \mathrm{nm}$ to $676.4\ \mathrm{nm}$) lasers. Gas lasers produce plasma lines that differ from the main lasing line. While being weak they can still cause problems and therefore filters must be used to remove them. Solid state lasers include Nd:YAG and diode lasers. When pulsed they and excimer lasers are used more specifically for time-resolved and ultraviolet resonance Raman spectroscopy. Nd:YAG lasers require pumping. For that older versions use flash-lamps while newer use an array of diode lasers ($800\ \mathrm{nm}$ to $900\ \mathrm{nm}$). The Nd:YAG laser has a primary lasing wavelength of $1064\ \mathrm{nm}$ which makes it very suitable for FT-Raman systems operating in the near-infrared region. Wavelength

of the $\mathrm{Nd{:}YAG}$ laser can be altered using frequency multiplication crystals that reduce the wavelength to one-half, -third or -fourth of the original. Diode lasers produce specific wavelength from the blue to the infrared region. Their advantages are small size and high efficiency with low power and cooling. Since they are very temperature sensitive they require precise controlling. Otherwise their wavelength and mode do not stay constant. Dye lasers are tunable lasers that can emit a wide range of wavelegths. They are pumped by a CW gas laser, a pulsed laser or a flashlamp. Dye lasers require large volumes of organic dye solutions. Also a tunable solid state laser using a titanium-sapphire crystal exists. It is tunable from $700\ \mathrm{nm}$ to $1030\ \mathrm{nm}$. [44, p.97–102]

Sample optics are used to illuminate the sample and collect the scattered light in the most efficient way. Due to the weak intensity of Raman scattering focusing of the incident beam and collecting of the scattered light properly is important. Common scattering geometries include $90\ \mathrm{deg}$ and $180\ \mathrm{deg}$. Mirrors and lenses are the most common optical components but optical fibres and metal probes have gained popularity recently. Pre-monochromators and filters are introduced to the system because of plasma lines of gas lasers and luminescence of semiconductor lasers. Filtering is needed because of the dependency between the frequencies of excitation and Raman scattered light. Multiple frequency illumination leads to multiple frequency scattering which decreases the signal-to-noise ratio of the measured Raman spectrum. A small aperture can also be added to block any environmental light from reaching the sample. Since lasers have high energy density attennuators must be used to prevent the sample being damaged by the heat created. Polarizator is needed if one wishes to measure polarized spectra. The collection system must be designed so that its aperture is large enough to receive as high portion of the scattered light as possible while minimizing light from other sources. Therefore again different optical filters are used. These include narrow band, notch and edge filters and also pre-monochromators. Filters are needed to reduce the intensity of Rayleigh scattered light to a minimum since it is higher than the intensity of Raman scattered light by several orders of magnitude. Scattered light requires its own polarizer if the intention is to measure polarized spectra. Raman microscopes are normally

confocal which means that the object point and the image point conjugate each other on the optical axis. It is the only way to achieve an ideal aberration-free optical image. Plane and depth resolution is greatly enhanced this way compared to non-confocal systems. [44, p.103] [46, p.59–63]

The spectral dispersion unit decomposes the scattered light spatially with energy. Its main components include enterance and exit slits, a collimator, a converging lens and one or multiple diffraction gratings. The collimator turns the light coming through the enterance slit into a more parallel-like beam that is uniformly distributed to the diffraction grating. The converging lens which can be a lens or a mirror converges the dispersed light at the exit slit. Aluminum plated mirrors are more commonly used than glass lenses due to their wider passband. [46, p.63–65]

2.6.3 Raman Spectroscopy of DNA

Raman spectra of DNA bases are illustrated for example in a reference database published in the *Journal of Raman Spectroscopy* [47]. The spectra from the article are shown in figure 6. The strongest peaks originate from ring breathing vibrations and are visible from $600\ \mathrm{cm}^{-1}$ to $800\ \mathrm{cm}^{-1}$. Thymine also has a prominent band at $1671\ \mathrm{cm}^{-1}$ due to ν(C=O) stretch vibrations. Medium strength and weak bands are visible from approximately $400\ \mathrm{cm}^{-1}$ to $1700\ \mathrm{cm}^{-1}$. The spectra of different DNA bases are in general easily distinguishable.

3 Materials and Methods

3.1 Sample Preparation

Single crystal silicon chips coated with thermally grown oxide layer were used as a basis for samples in this work. The chips were cut from a spherical wafer using a diamond cutter. Nominal size of the chips was aimed to be around $8\ \mathrm{mm}\times 8\ \mathrm{mm}$ but it was not particularly important. Upper limit for physical dimensions was kept at $10\ \mathrm{mm}\times 10\ \mathrm{mm}$ because bigger samples would not have

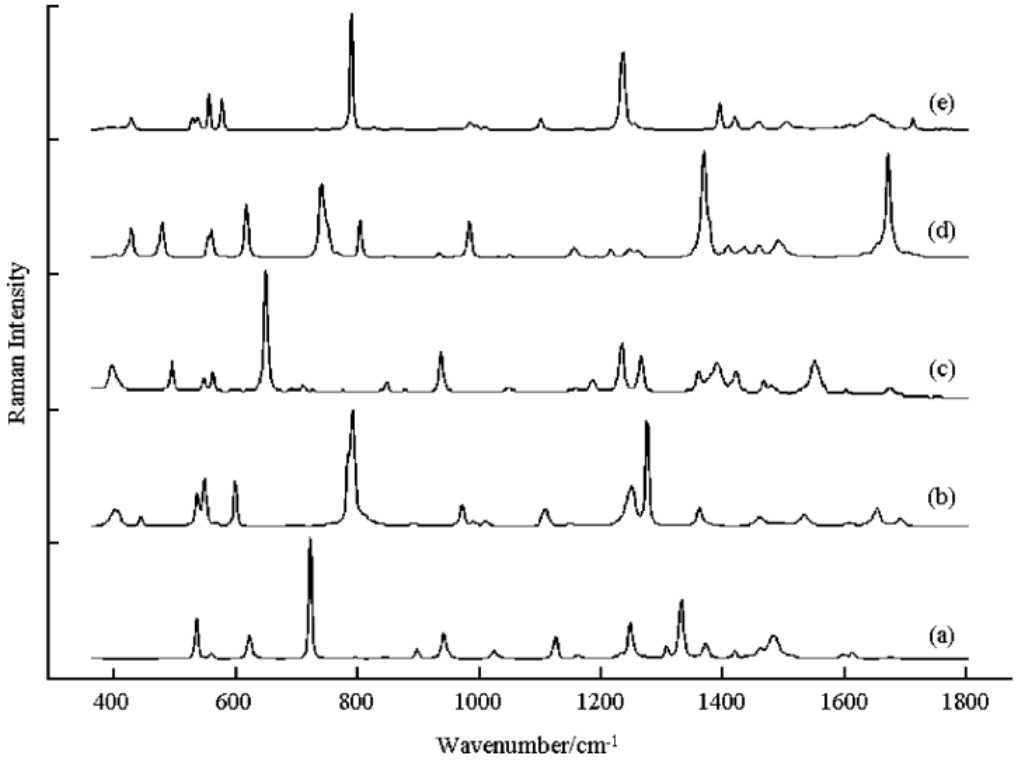

Figure 6: Raman spectra of DNA and RNA bases: (a) adenine, (b) cytosine, (c) guanine, (d) thymine and (e) uracil [47]

been practical. The chips were cleaned after the cutting by dipping them first in acetone and sonicated with ultrasound. If necessary cotton sticks were used to get rid of fingerprints for example. Then the chips were rinsed with isopropanol (IPA) to remove the acetone. Lastly nitrogen gas was used to dry the chips.

Next step was to coat the chips with a resist layer. A2 950 PMMA was chosen because it had been succesfully used in other similar projects. Thickness of the coated layer was roughly $100\ \mathrm{nm}$ and it was achieved by using the spin speed of 1500 rpm for $50\ \mathrm{s}$. After the spinning the resist was baked on a hot plate at $160\ ^{\circ}\mathrm{C}$ for five minutes.

The pattern for the electrodes was designed so that the Raman signal obtained later on would be reasonably strong while keeping the exposure time practical.

In order to achieve this a large array of fingertip electrodes was designed. The array consisted of three rows of fingertips two of those being used for trapping and one as a reference with no potential difference between the tips. Width of the smallest features and the length of the gap between the tips were patterned to be $100\ \mathrm{nm}$. The achieved gap size varied a bit but was acceptable if it remained under $200\ \mathrm{nm}$. Also a more simple and already tested single row pattern was used as well. Both patterns are illustrated in figures 7 and 8. The exposure of the pattern was performed using electron beam lithography (EBL). $30\ \mu\mathrm{m}$ aperture was used for the array and $120\ \mu\mathrm{m}$ for the contact pads and leads. Different step sizes were tested before fabricating real samples and in the end $10\ \mathrm{nm}$ was chosen for the main array part and $220\ \mathrm{nm}$ for the leads and contact pads. Area dose of $300\ \mu\mathrm{As/cm^2}$ was used for every element. The exposure time for one sample was approximately twenty minutes and it was done with *Raith eLiNE*. Samples were developed submerging them in a MIBK(Methyl isobutyl ketone)/IPA (3:1) solution for thirty seconds and then in IPA while also rinsing them with IPA. Samples were dried with nitrogen gas. After developement the samples were cleaned gently with an oxygen plasma flash using *Oxford Instruments Plasmalab 80 Plus* reactive ion etcher. The metal electrodes were then evaporated on top the chip with an e-beam evaporator. A titanium layer of $2\ \mathrm{nm}$ was evaporated first to ensure good adhesion of the $25\ \mathrm{nm}$ thick gold electrodes. The samples were also imaged with *Raith eLiNE* to ensure good quality of the gaps and cleaned with oxygen plasma after the lift-off to make the sample surface hydrophilic and remove any remaining resist residues.

3.2 Trapping of oligonucleotides

Single-stranded 40 bp ($14\ \mathrm{nm}$) were bought from *Integrated DNA Technologies*. They were modified with a thiol group attached to one end and a Cy3 dye molecule to another. The Sulfur atom in the thiol group would make a covalent bond with a gold atom in the electrode and the dye molecule would provide fluorescence. The oligonucleotides had a poly(CT) sequence meaning they consisted only of cytocine and thymine. Since these nucleobases do not create hydrogen bonds with each other the individual oligonucleotides do not make

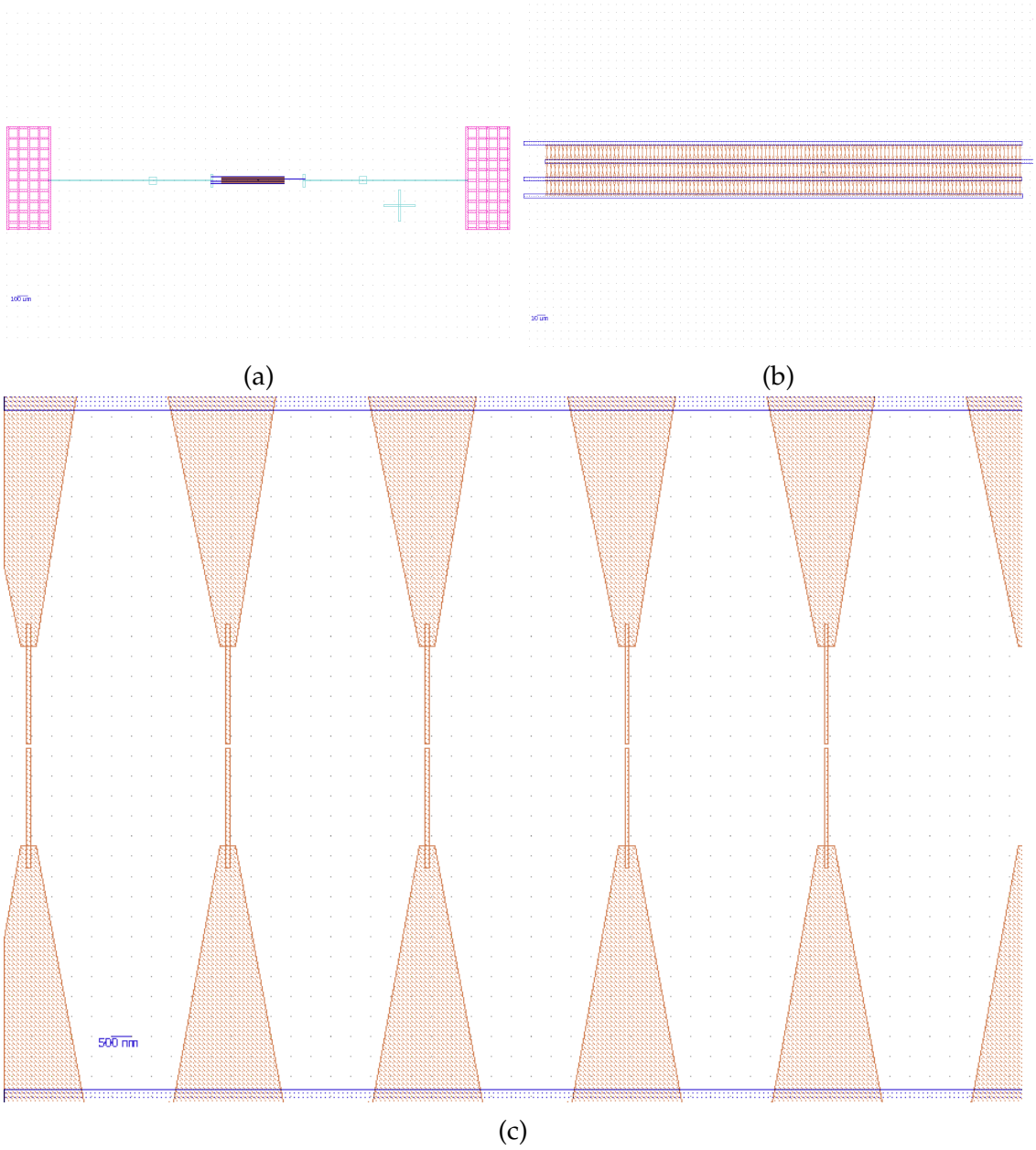

Figure 7: The Array pattern of the fingertip electrodes. (a) The whole structure including the large pads for external connection, leads and the array. (b) A more closer look at the array displaying the individual rows and leads. (c) Individual electrode pairs where the width and gap between the smallest features is 100 nm.

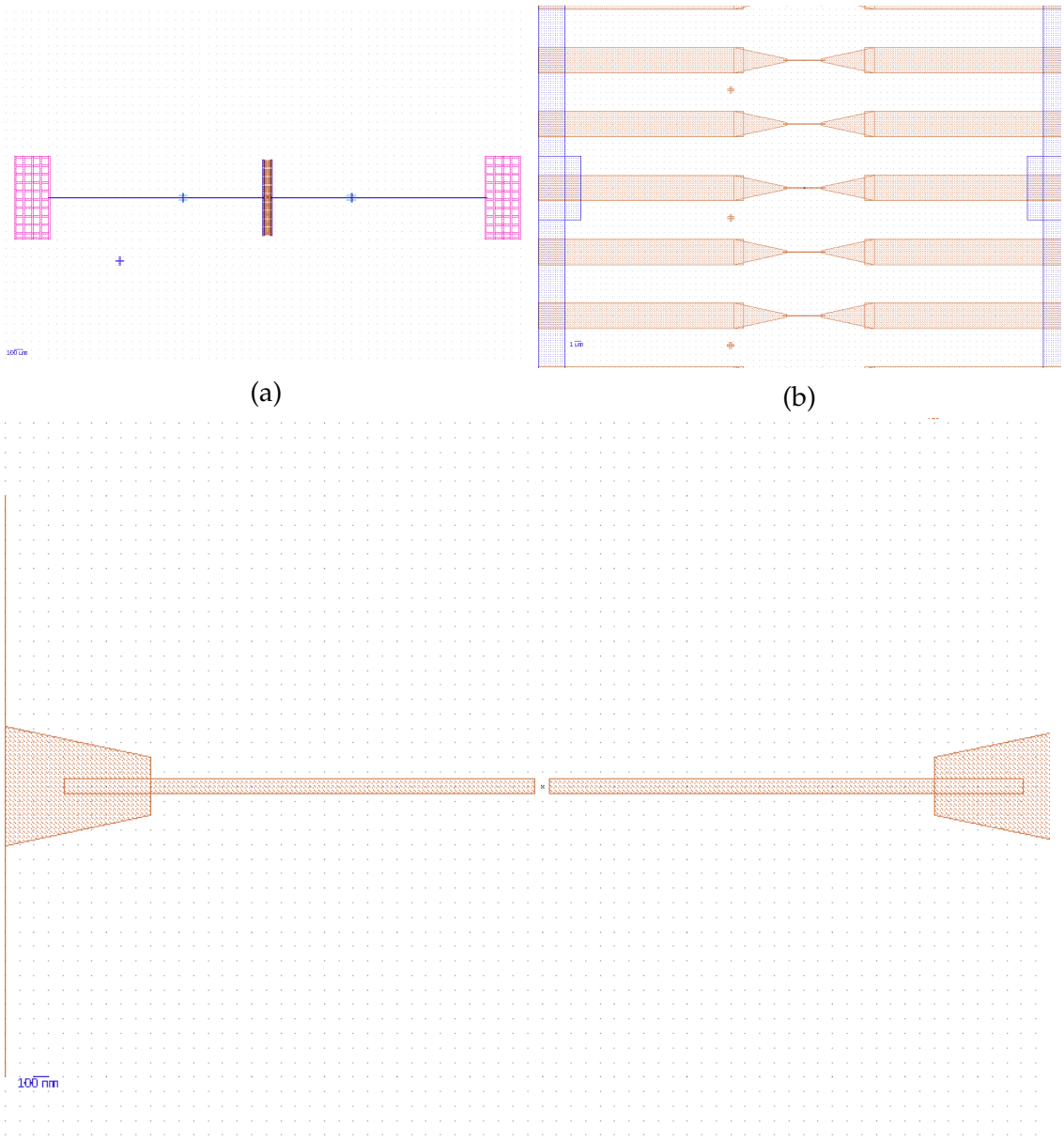

Figure 8: The single row pattern the fingertip electrodes. (a) The whole structure including the large pads for external connection, leads and the row of electrodes. (b) A more closer look at the row displaying the structure of the fingers. (c) A single electrode pair where the width and gap between the smallest features is $100\ \mathrm{nm}$.

bonds with themselves or other oligonucleotides. 7.5 pH Hepes ($3\ \mathrm{mM}$)/NaOH ($2\ \mathrm{mM}$) solution was used as a buffer.

For 'blind trapping' the sample was first attached to a stage where leads were connected to the pad electrodes of the sample. Then the stage was put into a closed box to protect the dyes from bleaching due to exposure to the ambient light. The other ends of the leads were connected to the box and further to a signal generator. From 10 µl to 12 µl of approximately $25\ \mathrm{nM}$ HEPES/NaOH buffered solution was pipetted on top of the sample. The number of oligos in one droplet is therefore approximately

$$N = N_A c V = 6.022 \cdot 10^{23}\ 1/\mathrm{mol} \cdot 25\ \mathrm{nmol/l} \cdot 12\ \mu\mathrm{l} = 1.8066 \cdot 10^{11}\ \approx 180 \cdot 10^9$$

where N_A is the Avogadro constant, c the molar concentration of the solution and V the volume of the droplet.

An AC signal of $5\ \mathrm{V}$ peak-to-peak voltage and a frequency of $1\ \mathrm{MHz}$ was applied between the electrodes from two to five minutes. The sample was then rinsed with 1000 µl of sterilized water and dried with nitrogen gas. Initial trapping parameters were the same used in an earlier trapping study [23] conducted in the same research group.

For live trapping under the confocal microscope the trapping parameters remained the same but the rig was different. Pieces of copper tape were glued to opposing sides of a glass sample plate with epoxy. Leads for the signal generator were soldered to the pieces. The sample was attached to the plate with *Scotch Tape* and connectors were bonded between the pads and the copper pieces. A drop of solution was again pipetted onto the sample and a coverplate was taped on top of that. The purpose of the tape was twofold. It naturally prevented the sample from moving but also acted as a spacer between the surface and the coverplate to create a large enough volume for the DNA solution.

3.3 Imaging and spectroscopy

The samples were studied under an *Olympus Fluoview 1000* confocal microscope after or during (in live trapping) the trapping. One channel was used to

see the reflection of the sample and another to obtain a fluorescent image. Both of these tasks were done with a $543\ \mathrm{nm}$ laser beam. Absorption peak of Cy3 is at $550\ \mathrm{nm}$. The detection range of the first channel was set to be from $544\ \mathrm{nm}$ to $554\ \mathrm{nm}$. A high pass filter was used to allow wavelengths above $560\ \mathrm{nm}$ to be detected in the second channel. A mirror was used to collect all of these wavelengths. The detection range of the second channel was automatically set from $555\ \mathrm{nm}$ to $655\ \mathrm{nm}$ which covers the emission range of Cy3 very well. Cy3 has an emission peak at $570\ \mathrm{nm}$. Emission and absorption spectra are depicted in figure 9

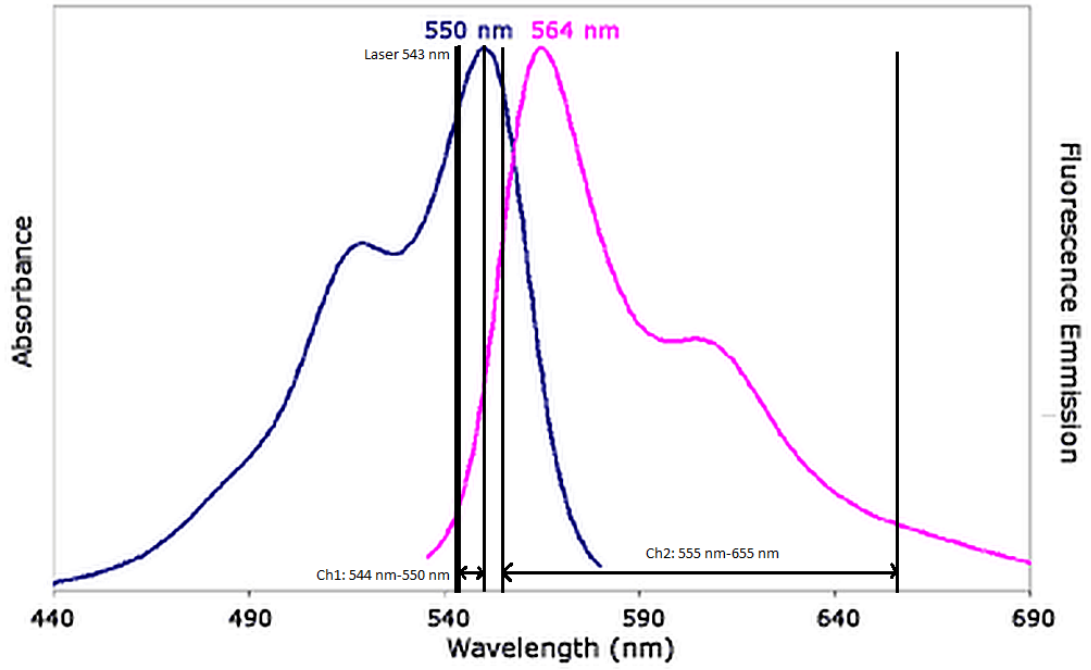

Figure 9: Cyanine 3 absorption and emisssion spectra [48]. In the image detection ranges of the two channels are shwon. Ch1 ($544\ \mathrm{nm}$ to $554\ \mathrm{nm}$) is set to receive some of the the laser light scattered of the sample while Ch2 ($555\ \mathrm{nm}$ to $655\ \mathrm{nm}$) is used for capturing the fluorescent light. The wavelength of the laser ($543\ \mathrm{nm}$) is also marked as vertical line. Absorption spectrum of the Cy3 is coloured in blue while the emission spectrum is colured in magenta.

Dry blind trapping samples were imaged with 60X air objective and wet live

trapping samples with 60X water immersion objective. Also digital zooming was used in addition since optical magnification of a 60X objective was not adequate alone. The reason for using a water objective with wet samples was to reduce the number of optical interfaces in the imaging setup. A 100X oil objective was also available but using it would have required applying a drop of oil on top of the sample plate which proved to be rather messy.

Raman measurements were done with a Bruker SENTERRA dispersive raman microscope. Wavelength of the laser was $758\ \mathrm{nm}$. Two spectra were measured from a sample. The background signal was measured from an area with no oligonucleotides. The actual desired signal was measured from the center of gap between one of the electrode pairs.

Some of the blind trapped samples were also studied with a scanning near field optical microscope (SNOM) and an atomic force microscope (AFM) to see if they gave different results compared to fluorescence imaging. The AFM operated on tapping mode, and height, amplitude and phase maps were measured. SNOM setup used two green lasers differing slightly in power and wavelength compared to the $543\ \mathrm{nm}$ laser used with the confocal microscope.

4 Results and discussions

4.1 Electrode fabrication

The sample preparation process did not yield any significant surprises or problems. Quality of the initial test samples was rather rough though. Since there are several steps in the lithography process some time was needed to fine-tune the parameters. Examples of early samples are presented in figures 10 and 11. Roughness was thought to be caused by the lift-off phase of the process. In order to fix this issue thickness of the resist layer was increased and the lift-off itself was done more aggressively by injecting acetone to the surface of the chip with a syringe. This way the lift-off could be done in a few minutes. Originally the chips were left in acetone for several hours without actively speeding up the process. Stepsize of the exposure was halved to ensure smoothness of the

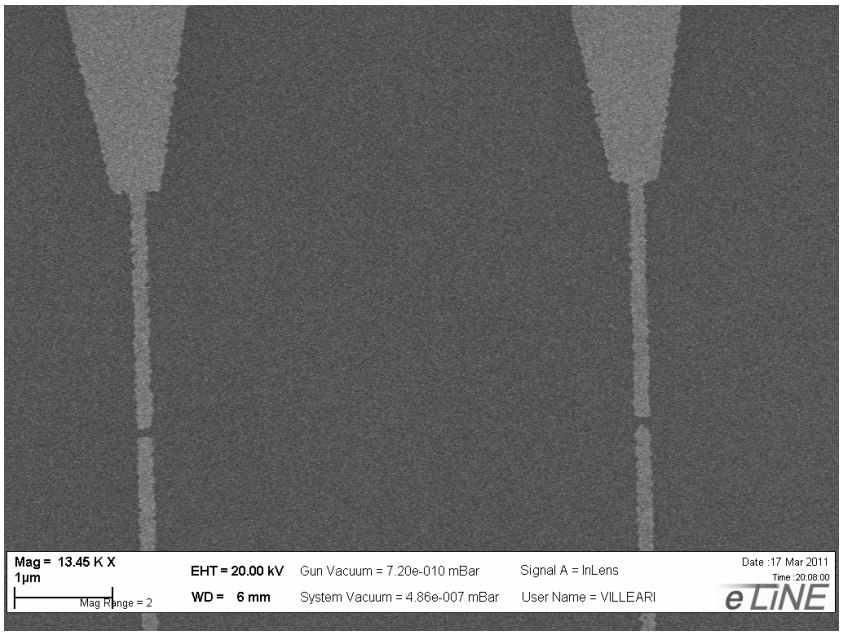

Figure 10: Roughness in an early stage sample. The edges of the fingertip electrodes are clearly jagged. Quality of the larger features is not as important but unnecessary roughness is still undesirable. Step size for this case has been $20\ \mathrm{nm}$

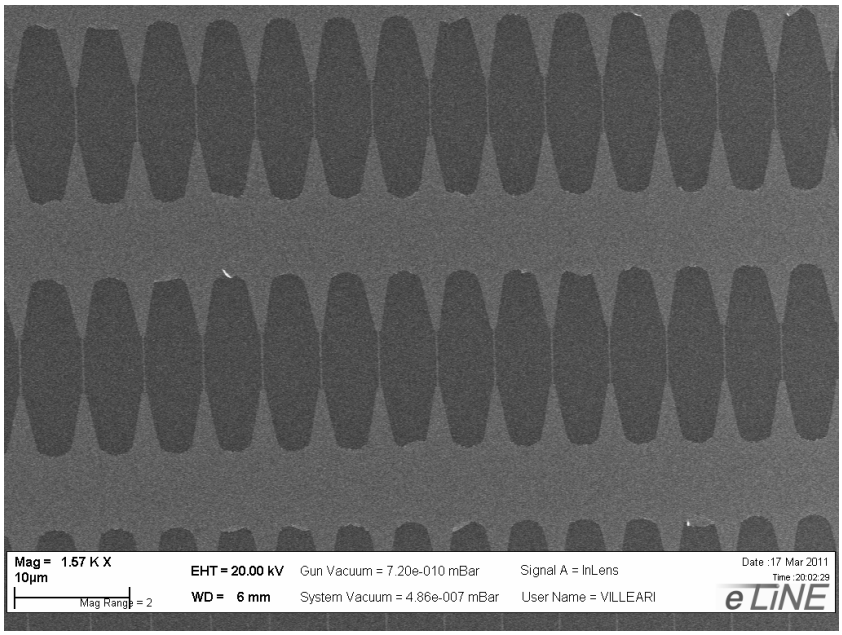

Figure 11: This image is from the same batch as figure 10 and shows that even the leads of the electrodes have jagged edges. Strips of the thin film can be seen dangling on the leads.

edges and sharpness of the corners of the pattern. Evaporation rate of Ti was increased since it has been seen experimentally that it improves the adhesion of Ti. Au behaves the opposite way so evaporation rate for that was decreased. Better film quality makes the lift-off easier. It is also quite obvious that the practical skills of yours truly got better sample by sample. An example of a later sample is presented in figure 12.

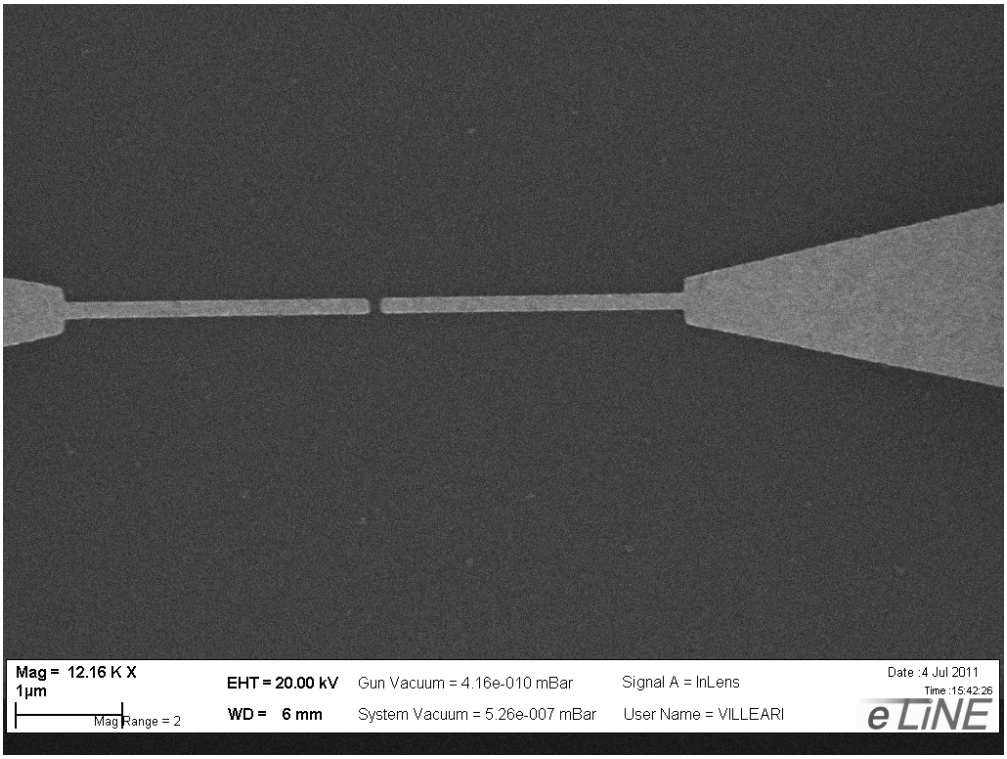

Figure 12: A better quality sample fabricated using a step size of 10 nm. The edges of the features are much more smooth compared to early test samples. Thickness of the resist layer has been increased a bit and lift-off has been conducted more rapidly.

4.2 Trapping

Trapping of the oligonucleotides can be considered a routine task since it has been done in the *Molecular Electronics and Plasmonics* research group before and data from existing simulations and experiments was available for this work [22].

Despite that trapping and imaging following it proved to be a quite challenging. Preparing the samples and the blind trapping itself were very straightforward as a procedure. The confocal microscope imaging was problematic however. Blind trapped samples did not yield any noticeable fluorescence between the electrodes. Electrical connections in the trapping setup were examined but no errors were found. Changing the trapping parameters or concentration of the solution did not help. In the process of solving this mystery one blind trapped sample using the old single row electrode pattern was imaged with an atomic force microscope. The results are shown in figure 13. There clearly is DNA visible thus proving the trapping had been successful. Somehow the fluorescence still could not have been seen. Live trapping results were different. At first only

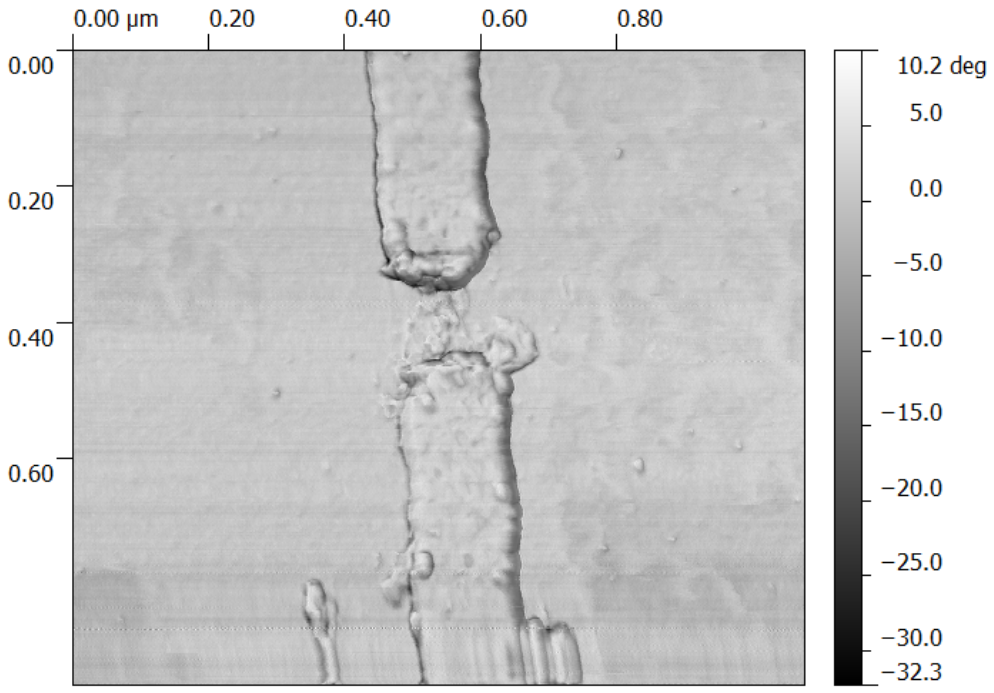

Figure 13: A phase image of a dry sample with blind trapped oligos in the gap between the electrodes.

the background noise was seen in the fluorescence channel. Even increasing the trapping voltage to ridiculously high values and switching the signal from AC to DC did not change anything. The voltage was so high that it should

have destroyed the electrodes which did not happen. This was due to faulty wiring. There was no potential difference whatsoever between the electrodes. Blind trapping did not have this problem because that very wire was only used with live trapping. Resoldering the faulty wire fixed the problem with the trapping itself. However the electrodes were destroyed due to excessive voltage before any fluorescence was seen in the gaps 14. Although nothing could have

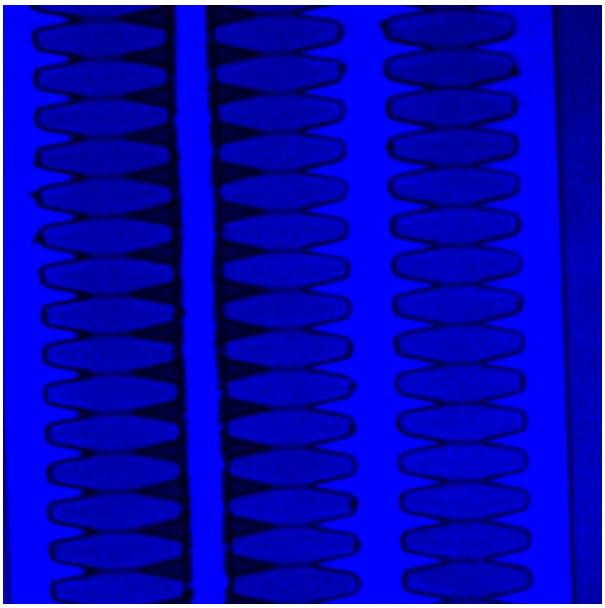

Figure 14: Destroyed electrodes of a sample using the array pattern. The electrodes have been melted due to the excessive voltage of the trapping signal.

been seen between the electrodes a strong signal was observed on top of the contact pads in the points where the solderings of the chip were 15. So at least the oligos were concentrating to some points and the dyes were working. Because of the problems encountered with both blind and live trapping a patch of new fresh oligos were bought from *Integrated DNA Technologies*. Also only the single row electrode pattern was used with the new oligos. At first the oligos did not yield different results but finally after adjusting the imaging parameters more thoroughly fluorescence was suddendly seen. Apparently increasing the digital zoom of the imaging system helped quite a lot which seems counterintuitive since it reduces the actual resolution. An example of a successful imaging effort is presented in figure 16.

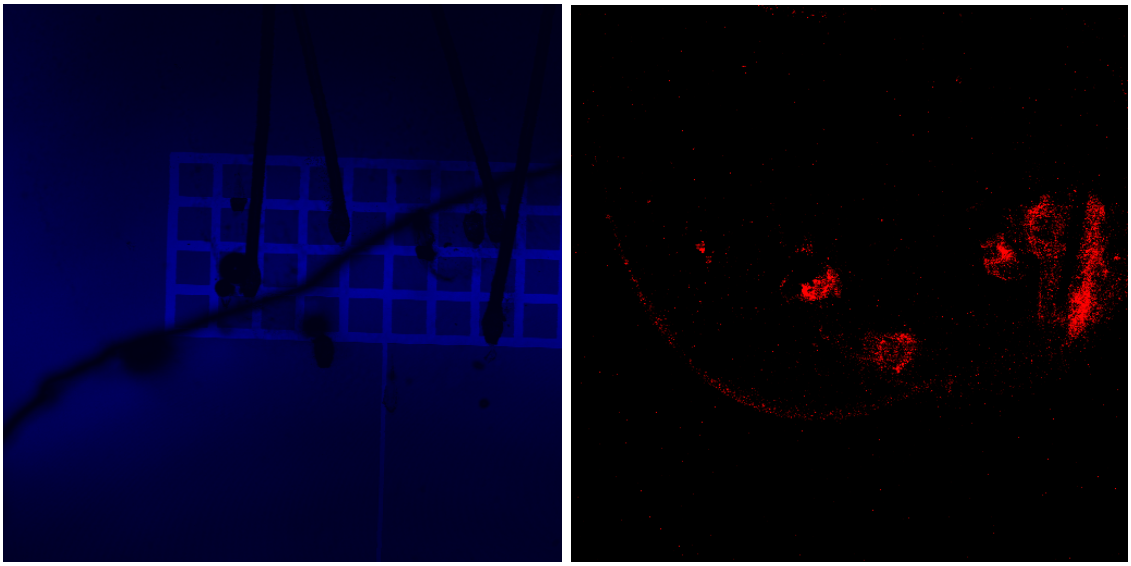

(a) Scattering channel (b) Fluorescence channel

Figure 15: (a) Scattering channel showing the contact pad and the bonded wires connecting it to the voltage source. (b) Fluorescence channel showing the accumulation of the oligos on the pad where the wires are bonded.

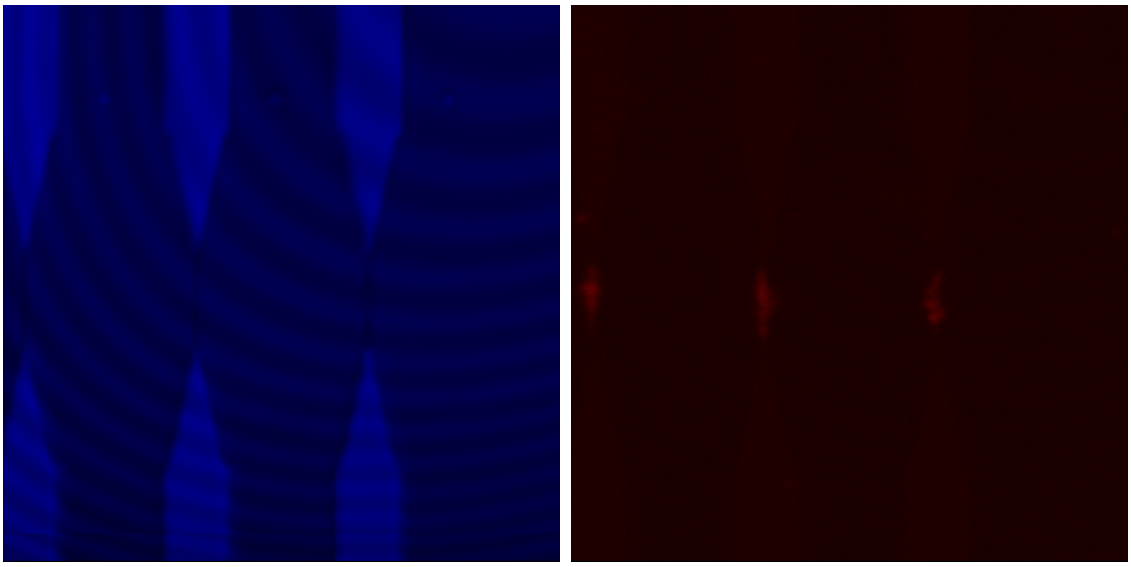

(a) Scattering channel (b) Fluorescence channel

Figure 16: (a) Scattering channel showing the electrodes. Diffraction patterns are also visible. (b) Fluorescence channel showing immobilized DNA oligos in the gap between the electrodes and also parallel to them.

4.3 Raman microscopy

Positive results from the AFM measurements and fluorescent imaging enabled the possibility to try to obtain a Raman spectrum of the sample. Those measurements confirmed that the trapping worked using the suggested and tested parameters and that the dyes were alive meaning any further problems would be related to the Raman setup itself. The microscope in question was however designed to detect only microscale objects at best. Since the oligos belong to the nanoscale results were not guaranteed and not so surprisingly the desired raman signal could not be obtained using the equipment at hand. Only one sample was measured but it was clear that more sophisticated tools were required to see something. The plot of the measurement is presented in figure 17 in which the three emission peaks come from the silicon substrate of the sample.

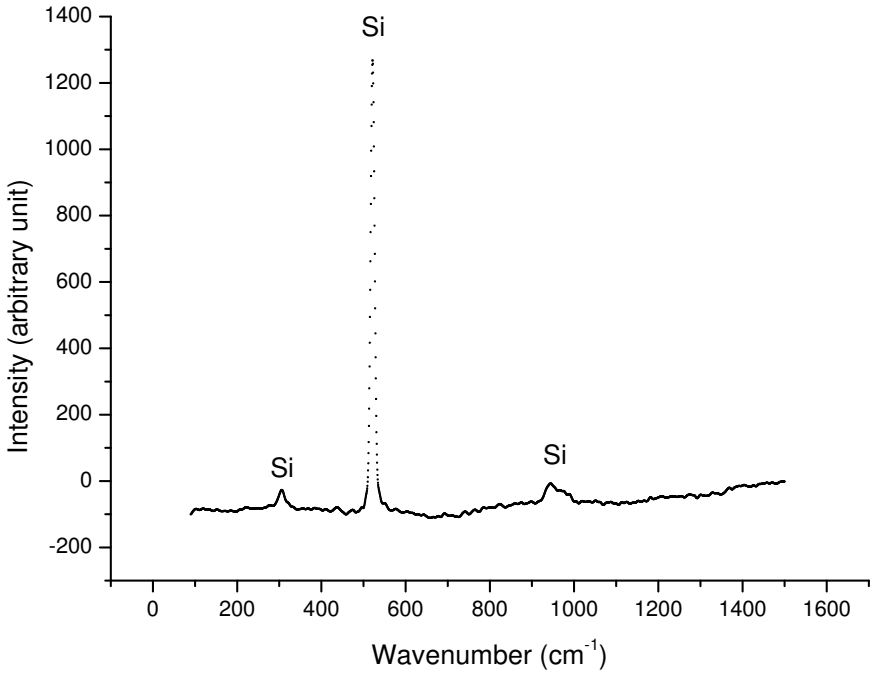

Figure 17: Raman spectrum of the measured sample. The Three peaks visible are originating from the silicon substrate [49].

5 Discussion and conclusions

The results are partly what was expected but also somewhat surprising. Nanofabrication methods such as electron beam lithography are well established in general and only little tweaking was required to achieve high enough quality samples. These basic methods are easily tunable for different types of electrode arrays suitable for trapping various nano- and microscale particles. An electrode array with integrated nanofluidistic channels could lead to a lab-on-a-chip solution which might have interesting applications in bio sciences for example.

Dielectrophoresis as a physical phenomenon originates from the 1950s and theory behind it is known. With that information it is relatively straightforward to make simulations and experimentally find the right parameters for different trapping scenarios. Trapping parameters used in this study were already used succesfully before and because of this it was first surprising to run into trouble when trapping the oligos. However the reason for fluorescence yields lower than expected was more likely the confocal microscope setup itself and differences in the oligos between this study and the reference [24] used. In this study there was only one dye molecule in the other end of the oligo unlike the reference that contained several dye molecules. Maybe the more significant reason was the bad alignment of the lasers in the confocal microscope setup. The setup is used in physical chemistry and cellular- and molecular biology research in addition to projects that are more on a physical side of nanoscience. Cellular-level spectroscopy does not require as much resolving power as was needed in this study which means other groups using the setup did not have any problems. They might have experienced some minor drops in yields but have not really been bothered by it. Because nobody had complained about their yields it was logical to start the search for the reason somewhere else. It may also make sense to blame the homemade trapping setup or parameters instead of a commercial confocal microscope hardware. The bad alignment may have also induced bleaching of the dyes because higher laser powers were used to compensate the low yields. Bleaching reduced the already low yields and made it almost impossible to see anything. The microscope was serviced afterwards and the alignment was fixed but new attempts to get better yields were not done since

the fluorescence spectroscopy was not the main objective of this study. It was eventually enough to at least obtain some kind of yields.

Cy3 is a long-wavelength dye that is commonly used in fluorescence microscopy and nucleic acid-based detection. Its characteristics are therefore well-known. There are however other Cy3-like dyes that are spectrally comparable to it meaning they have similar absorption and emission maxima, Stokes shifts, and extiction coefficients. This Cy3-like group includes Alexa Fluor 555, DY-550 and Atto 565 for example. Alexa Fluor dyes in general are considered to be more resistant to fluorescence quenching and photobleaching than Cy3 and other aforementioned Cy3-like dyes. [50] In a study comparing Alexa Fluor and CyDye for DNA microarray use Cy3 and Cy5 exhibited significantly higher intensities and signal-to-noise ratios than their Alexa Fluor counterparts while being less stable photochemically [51]. Since the DEP trapping and imaging of the results was fairly quick the increased photostability of Alexa Fluor dyes could be considered unnecessary. Strong signal intensity is more important when doing measurements in nanoscale, especially with equipment that is not in its optimal condition.

The confocal microscope was equipped with a diode laser ($405\ \mathrm{nm}$), multiline Argon-laser ($458\ \mathrm{nm}$, $488\ \mathrm{nm}$, $514\ \mathrm{nm}$) and two $\mathrm{He-Ne}$-lasers ($543\ \mathrm{nm}$, $633\ \mathrm{nm}$). Therefore many spectrally different dyes could have been used. Those include for example cyanine-like DY-550 (absorption peak at $553\ \mathrm{nm}$), Alexa Fluor 555 ($555\ \mathrm{nm}$), Atto 565 ($561\ \mathrm{nm}$), DY-630 ($630\ \mathrm{nm}$), Alexa Fluor 633 ($632\ \mathrm{nm}$), DY-635 ($634\ \mathrm{nm}$), Cy5 ($649\ \mathrm{nm}$), Alexa Fluor 647 ($650\ \mathrm{nm}$). [50] Other spectrally compatible dyes include PIH ($536\ \mathrm{nm}$), EtBr ($520\ \mathrm{nm}$), PicoGreen ($503\ \mathrm{nm}$), SYBR Gold ($496\ \mathrm{nm}$), SYBR Green I ($498\ \mathrm{nm}$), Yoyo-1 ($490\ \mathrm{nm}$). [52] However as alredy mentioned Cy3 was considered to be a safe choice because of its common use and well-known characteristics.

Raman spectroscopy of the trapped oligos was ultimately the main goal. It was known beforehand that it might not work as planned. In this case a clear good signal from the oligos could not be obtained. The reason is not likely to be a fundamental but more of a technical problem. With a similar setup with more resolving power one probably could obtain a good signal. Other option would

be to try some kind of a near-field Raman setup.

A study published already in 2000 shows that fluorescent DNA can be detected using a SNOM [53]. In the study $48.5kbp$ λ DNA molecules in 5 $\mu\mathrm{M}$ solutions with $500\ \mathrm{nM}$ and 5 $\mu\mathrm{M}$ YOYO-1 buffered in $10\ \mathrm{mM}$ Tris-HCl and $1\ \mathrm{mM}$ EDTA solution were detected using a 100X oil immersion lens. Because the study concerns fluorescence detection rather than Raman spectroscopy and it involves very large molecules compared to the ones used in this study it is not particularly interesting. However it still suggests that SNOM setups can be promising when biomolecules are studied. Another study shows that localized salt complexes in tetracyanoquinodimethane organic thin films can be detected with a $\sim 120\ \mathrm{nm}$ resolution using a SNOM-Raman setup without field enhancement effects [54]. Although not involving DNA the study shows SNOM-Raman setups can be viable options when one is trying to combine nanoscale DEP with Raman scattering. Surface-enhanced Raman (SERS) imaging of dye labeled DNA has in fact been achieved with $100\ \mathrm{nm}$ resolution using SNOM [55]. The technique is not label free though and what is actually measured is the Raman spectrum of the dye not the DNA itself. Because of that the setup in question is suitable for detection of the DNA but not direct characterization.

Some kind of field enhancement seems to be almost mandatory if one wants to measure Raman spectra of DNA in nanoscale. At least it is highly recommended to utilize it if possible. In addition to SERS tip-enhanced Raman scattering (TERS) brings interesting possibilities to the table [56]. The problem with SERS is that roughness and variation in shape and size of the particles and clusters that produce the field enhancement produce spatial variations in the observed Raman signal. As a result quantitative analysis cannot be done properly. This problem can be circumvented using a single metal nanoparticle in the form of a sharp tip working as a field enhancing site. The metal tip is scanned over the sample surface as in a scanning probe microscope resulting in a technique called TERS. The lateral resolution of this technique can be $10\ \mathrm{nm}$ and it therefore can give chemical and structural information on the sample with excellent lateral resolution and sensitivity. This is very beneficial in biosciences where certain biological effects can be very location specific. DNA is a very good ex-

ample of this. With TERS a single base sensitivity in characterization could potentially be reached. With SERS nucleobases are difficult to identify because the sugar and phosphate groups interfere with the signal. Because of that indirect detection using Raman-active dyes is often carried out. If TERS can work without labels it can be considered as an ultimate tool for Raman spectroscopy in nanoscale. As a further enhancement adiabatic tip-plasmon focusing can be used with TERS [57].

SERS and DEP have been combined with microfluidistic channels in the recent past [58] [59]. Field enhancing nanoparticles are suspended in microfluidistic channels with the particles of interest. DEP is used to localize the field enhancing particles to the electrodes in order to achieve local field enhancement while the flow of the particles is kept laminar and the flow rate optimal. The size of the electrodes in these setups is in the order of micrometres and the molar concentrations in micro moles per litre. It would be interesting to see if this worked in nanoscale also.

In a study published in 2014 $200\ \mathrm{nm}$ thick gold electrodes with the width and gapsize of $1\ \mu\mathrm{m}$ were fabricated on a glass wafer using photolithography and e-beam evaporation [60]. Au nanoparticles were trapped between the electrodes to form pearl chains with nanogaps between the adjacent particles. Analyte molecules and Au nanoparticles were drop-casted onto the electrodes and Raman spectra were obtained. The In Situ SERS setup used a $785\ \mathrm{nm}$ diode laser and a 50X objective (N.A. 0.55). Raman spectra were measured from benzenethiol and adenine solutions. Signals could be obtained from $2\ \mu\mathrm{l}$ samples of $1\ \mathrm{mM}$. However using a $752.5\ \mathrm{nm}$ Kr-ion laser and a one hour incubation of the solutions adenine could be detected from a sample having a concentration as low as $100\ \mathrm{fM}$.

In a another study published in 2014 proteins were trapped using DEP and their SERS spectra measured successfully [61]. An array of titanium electrodes with a gap size of $10\ \mathrm{nm}$, a width of a few hudred nanometres and a thickness of $40\ \mathrm{nm}$ was fabricated using electron beam lithography. Titanium was used instead of gold for example because gold can be prone to corrosion in electrolytes that contain chloride. Field enhancement for SERS was acquired from

the nanogaps. It was claimed that if the gap size is more than $10\ \mathrm{nm}$ nanogaps like this necessarily would not work as hotspots for SERS. For DEP an ac signal with frequencies from hudreds of kilohertz to $4\ \mathrm{MHz}$ and peak-to-peak voltages from $0.1\ \mathrm{V}$ to $15\ \mathrm{V}$ were used. The ac signal was also coupled with a dc bias from $10\ \mathrm{mV}$ to $100\ \mathrm{mV}$ for electronic detection of the molecules in the nanogaps. The molecules in question were r-phycoerythrin (RPE) which is a disk-shaped protein with a diameter of $11\ \mathrm{nm}$ and a thickness of $6\ \mathrm{nm}$. Final $0.8\ \mathrm{nM}$, $0.26\ \mathrm{nM}$ and $0.12\ \mathrm{nM}$ protein concentrations were created from RPE ($4.0\ \mathrm{mg/ml}$) and PBS buffer ($100\ \mathrm{mM}\ Na_2HPO_4$, $150\ \mathrm{mM}\ \mathrm{NaCl}$, pH 7.2). For confocal microscopy a $2\ \mu\mathrm{l}$ droplet of the solution was confined in a small fluidic chamber using adhesive tape. Raman spectra were measured using a confocal microscope with a $633\ \mathrm{nm}$ $\mathrm{He}-\mathrm{Ne}$ laser and 50X (N.A. 0.5) and 100X (N.A. 0.9) objectives. Obtained Raman signals were compared against an RPE sample measured with silver colloid hydrosol. As a result clear signals showing the most distinctive peaks was acquired.

As a conclusion DEP is a very useful and convenient method of localizing nanoparticles to a single spot for microscopy and spectroscopy. However some sort of field enhancement like SERS or TERS is in practise necessary when measuring Raman spectra of biomolecules such as DNA in nanoscale. If using the nanogap of the DEP electrodes as SERS hotspots $100\ \mathrm{nm}$ gaps most likely are too wide to work properly. Gaps of $10\ \mathrm{nm}$ on the other hand are narrow enough. Alternatively localized metallic nanoparticles trapped between the elctrodes also provide field enhancement. The best spatial resolution can be achieved with a near-field TERS setup but might not be suitable for applications that require more simplified and faster to use setups. Lab-on-a-chip samples could also be useful if DEP and nanofluidistics were combined.

References

[1] N. C. Seeman, *DNA in a material world*, Nature **421**, 427 (2003).

[2] P. W. K. Rothemund, *Folding DNA to create nanoscale shapes and patterns*, Nature **440**, 297 (2006).

[3] S. M. Douglas, H. Dietz, T. Liedl, B. Högberg, F. Graf, W. M. Shih, *Self-assembly of DNA into nanoscale three-dimensional shapes*, Nature **459**, 414 (2009).

[4] B. Saccà, R. Meyer, M. Erkelenz, K. Kiko, A. Arndt, H. Schroeder, K. S. Rabe, C. M. Niemeyer, *Orthogonal Protein Decoration of DNA Origami*, Angew. Chem. Int. Ed. **49**, 9378 (2010).

[5] N. V. Voigt, T. Tørring, A. Rotaru, M. F. Jacobsen, J. B. Ravnsbæk, R. Subramani, W. Mamdouh, J. Kjems, A. Mokhir, F. Besenbacher, K. V. Gothelf, *Single-molecule chemical reactions on DNA origami*, Nature Nanotechnology **5**, 200 (2010).

[6] R. G. Endres, D. L. Cox, R. R. P. Singh, *Colloquium: The quest for high-conductance DNA*, Rev. Mod. Phys. **76**, 195 (2004).

[7] D. Porath, G. Cuniberti, R. Di Felice, *Charge Transport in DNA-Based Devices*, arXiv:cond-mat/0403640v2 [cond-mat.mtrl-sci], (2004).

[8] S. Tuukkanen, A. Kuzyk, J. J. Toppari, V. P. Hytönen, T. Ihalainen, P. Törmä, *Dielectrophoresis of nanoscale double-stranded DNA and humidity effects on its electrical conductivity*, Appl. Phys. Lett. **87**, 183102 (2005).

[9] G. L. Liu, L. P. Lee, *Nanowell surface enhanced Raman scattering arrays fabricated by soft-lithography for label-free biomolecular detections in integrated microfluidics*, Appl. Phys. Lett. **87**, 074101 (2005).

[10] H. A. Pohl, *The Motion and Precipitation of Suspensoids in Divergent Electric Fields*, J. Appl. Phys. **22**, 869 (1951).

[11] H. A. Pohl, *Some Effects of Nonuniform Fields on Dielectrics*, J. Appl. Phys. **29**, 1182 (1958).

[12] A. Ashkin, *Acceleration and Trapping of Particles by Radiation Pressure*, Phys. Rev. Lett. **24**, 4 (1970).

[13] A. Ashkin, J. M. Dziedzic, J.E. Bjorkholm, S. Chu, *Observation of a single-*

beam gradient force optical trap for dielectric particles, Opt. Lett. **11**, 5 (1986).

[14] C. K. Mathews, K. E. van Holde, *Biochemistry* (The Benjamin/Cummings Publishing Company, Redwood City, 1990).

[15] `https://en.wikipedia.org/wiki/DNA`, 2016–3–17.

[16] T. M. Devlin, *Textbook of Biochemistry with Clinical Correlations* (Wiley-Liss, Inc., New York, 1997).

[17] G. M. Blackburn, M. J. Gait, D. Loakes, D. M. Williams, *Nucleic Acids in Chemistry and Biology* (The Royal Society of Chemistry, Cambridge, 2006).

[18] V. Linko, *DNA-Based Applications in Molecular Electronics*, Ph.D. thesis, University of Jyväskylä, 2011.

[19] R. Pethic, *Dielectric and Electronic Properties of Biological Materials* (John Wiley & Sons, Chichester, 1979).

[20] T. B. Jones, *Electromechanics of Particles* (Cambridge University Press, Cambridge, 2005).

[21] H. A. Pohl, R. Pethig, *Dielectric Measurements Using Non-Uniform Electric Field (Dielectrophoretic) Effects*, J. Phys. E: Sci. Instrum. **10**, 190 (1977).

[22] S. Tuukkanen, A. Kuzyk, J. J. Toppari, H. Häkkinen, V. P. Hytönen, E. Niskanen, M. Rinkiö, P. Törmä, *Trapping of 27 bp - –8 kbp DNA and immobilization of thiol-modified DNA using dielectrophoresis*, Nanotechnology **18**, 295204 (2007).

[23] V. Linko, J. Leppiniemi, B. Shen, E. Niskanen, V. P. Hytönen and J. J. Toppari, *Growing of immobilized DNA by polymerase: bridging nanoelectrodes with individual dsDNA molecules*, Nanoscale **3**, 3788 (2011).

[24] T. K. Hakala, V. Linko, A-P. Eskelinen, J. J. Toppari, A. Kuzyk, and P. Törmä, *Field-Induced Nanolithography for High–Throughput Pattern Transfer*, small **5**, 23 (2009).

[25] C. L. Ashbury, A. H. Diercks, G. van den Engh, *Trapping of DNA by dielectrophoresis*, Electrophoresis **23**, 2658 (2002).

[26] C.-F. Chou, J. O. Tegenfeldt, O. Bakajin, S. S. Chan, E. C. Cox, N. Darnton, T. Duke, R. H. Austin, *Electrodeless Dielectrophoresis of Single- and Double-Stranded DNA*, Biophys. J. **83**, 2170 (2002).

[27] S. Tuukkanen, J. J. Toppari, A. Kuzyk, L. Hirviniemi, V. P. Hytönen, T. Ihalainen, P. Törmä, *Carbon Nanotubes as Electrodes for Dielectrophoresis of DNA*, Nano Lett. **6**, 7 (2006).

[28] H. Häkkinen, *The gold-sulfur interface at the nanoscale*, Nat. Chem. **4**, 443 (2012).

[29] H. D. Young and R. A. Freedman, *University Physics with modern physics* (Addison Wesley Longman, San Francisco, 2004), *11th edition*.

[30] `http://www.intel.com/content/www/us/en/silicon-innovations/intel-14nm-technology.html`, 2014–11–02.

[31] Jeol Ltd, *Invitation to the SEM World*.

[32] L. Reimer, *Scanning Electron Microscopy, Physics of Image Formation and Microanalysis* (Springer-Verlag, Berlin Heidelberg, 1985).

[33] D. J. Stokes, *Principles and Practice of Variable Pressure/Environmental Scanning Electron Microscopy (VP-ESEM)*, edited by Mark Rainforth (John Wiley & Sons, Chichester, 2008).

[34] Jeol Ltd, *A Guide to Scanning Microscope Observation*.

[35] S. Franssila, *Introduction to microfabrication* (John Wiley & Sons, Chichester 2010), *2nd edition*.

[36] M. Stepanova, S. Dew, *Nanofabrication Techniques and Principles* (Springer-Verlag, Wien, 2012).

[37] S. Cabrini, S. Kawata, *Nanofabrication Handbook* (CRC Press, Boca Raton, 2012).

[38] `http://www.azonano.com/article.aspx?ArticleID=3219`, 2015–07–16.

[39] T. R. Corle, G. S. Kino, *Confocal Scanning Optical Microscopy and Related Imaging Systems* (Academic Press, San Diego, 1996).

[40] G. Palumbo, R. Pratesi, *Lasers and Current Optical Techniques in Biology* (The Royal Society of Chemistry, Cambridge 2004).

[41] U. Resch-Genger, M. Grabolle, S. Cavaliere-Jaricot, R. Nitschke, T. Nann, *Quantum dots versus organic dyes as fluorescent labels*, Nature Methods **5**, 9 (2008).

[42] M. Bruchez Jr., M. Moronne, P. Gin, S. Weiss, A. P. Alivisatos, *Semiconductor Nanocrystals as Fluorescent Biological Labels*, Science **281**, 2013 (1998).

[43] C. V. Raman, K. S. Krishnan, *A new type of secondary radiation*, Nature **121**, 3048 (1928).

[44] J. R. Ferraro, K. Nakamoto, C. W. Brown, *Introductory Raman Spectroscopy* (Academic Press, San Diego, 2003), *2nd edition*.

[45] `https://en.wikipedia.org/wiki/Raman_spectroscopy`, 2016–4–13.

[46] S.-L. Zhang, *Raman Spectroscopy and Its Application in Nanostructures*, (John Wiley & Sons, Chichester, 2012) *2nd edition*.

[47] J. De Gelder, K. De Gussem, P. Vandenabeele, L. Moens, *Reference database of Raman spectra of biological molecules*, J. Raman Spectrosc. **38**, 1133 (2007).

[48] `http://eu.idtdna.com/site/Catalog/Modifications/Product/1474`, 2015–07–16.

[49] `http://rruff.info/Silicon`, 2016–4–14.

[50] J. E. Berlier, A. Rothe, G. Buller, J. Bradford, D. R. Gray, B. J. Filanoski, W. G. Telford, S. Yue, J. Liu, C.-Y. Cheung, W. Chang, J. D. Hirsch, J. M. Beechem, Rosaria P. Haugland, Richard P. Haugland, *Quantitative Comparison of Long-wavelength Alexa Fluor Dyes to Cy Dyes: Fluorescence of the Dyes and Their Bioconjugates*, J Histochem Cytochem **51**, 12 (2003).

[51] J. L. Ballard, V. K. Peeva, C. J. S. deSilva, J. L. Lynch, N. R. Swanson, *Comparison of Alexa Fluor® and CyDye™ for practical DNA microarray use*, Mol Biotechnol **36**, 175 (2007).

[52] G. Cosa, K.-S. Focsaneanu, J. R. N. McLean, J. P. McNamee, J. C. Scaiano, *Photophysical Properties of Fluorescent DNA-dyes Bound to Single- and Double-stranded DNA in Aqueous Buffered Solution*, Photochemistry and Photobiology **73**, 6 (2001).

[53] H. Muramatsu, K. Homma, N. Yamamoto, J. Wang, K. Sakata-Sogawa, N. Shimamoto, *Imaging of DNA molecules by scanning near-field microscope*, Mater. Sci. Eng. C-Rep. **12**, 29 (2000).

[54] P. G. Gucciardi, S. Trusso, C. Vasi, S. Patanè, M. Allegrini, *Optical near-field Raman imaging with subdiffraction resolution*, Appl. Opt. **42**, 15 (2003).

[55] V. Deckert, D. Zeisel, R. Zenobi, *Near-Field Surface-Enhanced Raman Imaging of Dye-Labeled DNA with 100-nm Resolution*, Anal. Chem. **70**, 2646 (1998).

[56] E. Bailo, V. Deckert, *Tip-enhanced Raman scattering*, Chem. Soc. Rev. **37**, 921 (2008).

[57] S. Berweger, J. M. Atkin, R. L. Olmon, N. B. Raschke, *Adiabatic Tip-Plasmon Focusing for Nano-Raman Spectroscopy*, J. Phys. Chem. Lett. **24**, 1 (2010).

[58] A. F. Chrimes, K. Khoshmanesh, P. R. Stoddart, A. A. Kayani, A. Mitchell, H. Daima, V. Bansal, K. Kalantar-Zadeh, *Active Control of Silver Nanoparticles Spacing Using Dielectrophoresis for Surface-Enhanced Raman Scattering*, Anal. Chem. **84**, 4029 (2012).

[59] A F. Chrimes, A. A. Kayani, K. Khoshmanesh, P. R. Stoddart, P. Mulvaney, A. Mitchella, K. Kalantar-Zadeh, *Dielectrophoresis-Raman spectroscopy system for analysing suspended nanoparticles*, Lab Chip **11**, 921 (2011).

[60] S. Cherukulappurath, S. H. Lee, A. Campos, C. L. Haynes, S.-H. Oh, *Rapid and Sensitive in Situ SERS Detection Using Dielectrophoresis*, Chem. Mater. **26**, 2445 (2014).

[61] L. Lesser-Rojas, P. Ebbinghaus, G. Vasan, M.-L. Chu, A. Erbe, C.-F. Chou, *Low-Copy Number Protein Detection by Electrode Nanogap-Enabled Dielectrophoretic Trapping for Surface-Enhanced Raman Spectroscopy and Electronic Measurements*, Nano Lett. **14**, 2242 (2014).